A VIBRATIONAL STUDY OF A SERIES OF MATRIX-ISOLATED NITRATES

By

DONALD EUGENE SMITH II

Bachelor of Science

Oklahoma State University

Stillwater, Oklahoma

1966

Submitted to the Faculty of the Graduate College
of the Oklahoma State University
in partial fulfillment of the requirements
for the Degree of
DOCTOR OF PHILOSOPHY
May, 1971

A VIBRATIONAL STUDY OF A SERIES

OF MATRIX-ISOLATED NITRATES

Thesis Approved:

J. Paul Devlin
Thesis Adviser

Neil Purdie

Lionel M. Raff

James Lange

D. D. Durham
Dean of the Graduate College

ACKNOWLEDGEMENTS

I would like to take this opportunity to express my appreciation for the guidance, patience and assistance provided by my adviser, Dr. J. Paul Devlin. Acknowledgement is also due Dr. D. W. James for a number of enlightening discussions relative to this research. I would also like to thank my wife, Kay, for her encouragement and understanding throughout my tenure in graduate school.

I would like to express my gratitude to the National Science Foundation, and Oklahoma State University Research Foundation for their support of this project.

Finally, I would like to extend my thanks to Wayne Adkins, our scientific glassblower, and Heinz Hall, and his fellow machine shop workers, for their assistance in design of the equipment used in this research, and their expertise in constructing it.

TABLE OF CONTENTS

LIST OF TABLES

LIST OF FIGURES

LIST OF FIGURES (Continued)

CHAPTER I

INTRODUCTION

Vibrational spectroscopy has been shown time and time again to be one of the most powerful methods known for the elucidation of molecular structure. However, there are times when the conventional sample-preparation techniques are not suitable. For example, the study of highly reactive or unstable species and high temperature species is experimentally very difficult. The study of intermolecular interactions in dilute systems may be hampered by lack of a suitable solvent, uncertainties in solute-solvent interactions or interfering solvent vibrational frequencies. It was to handle just these types of problems that the technique of matrix isolation was developed.

The Problem

This investigation will be directed toward obtaining vibrational spectra of a series of monomeric nitrates. These results will be compared and correlated with data obtained from crystalline and melt systems, and with some relevant normal coordinate calculations.

The nitrates were chosen for this investigation because of the interest in the nitrate ion as a probe of ionic environments, where results have been interpreted according to models imposing various perturbations on the nitrate ion. The results of this study will be applied to a discussion of the validity of these models. It is well known that the

asymmetric N-O stretching mode is quite intense in the Raman spectrum. Thus the nitrates are experimentally advantageous in that at least part of the Raman spectrum should be detectable even at high dilution.

The experimental phase of this study involves the assembly of the laser Raman apparatus, design and assembly of a matrix isolation cryostat suitable for infrared and Raman investigations, preparation of the films of nitrates in such dilution as to insure the presence of monomeric species isolated in an inert environment, and the examination of the infrared and Raman spectra of these films.

Matrix Isolation

The technique of matrix-isolation was originally developed by Pimentel[1] and coworkers for the study of infrared spectra of unstable free radicals. Since then a considerable amount of research has been carried out using this technique, involving not only free radicals, but many other molecular species as well. The matrix-isolation technique offers an extremely powerful tool in the study of intermolecular interactions.

The general technique of matrix-isolation consists of dispersion of an active species, A, in a chemically inert matrix, M, at temperatures sufficiently low to prevent diffusion of the active species, an at sufficiently high M\A ratio to preclude A-A intermolecular interactions. The matrix material must, in most cases, be nonreactive with the active species, and reasonably transparent in the spectral region of interest. The most commonly used matrix materials are nitrogen and rare gases. With these materials one must, therefore, work at liquid hydrogen or helium temperatures so that the matrix is sufficiently rigid to prevent

diffusion of the active species. M/A ratios in excess of 300/1 are normally required.

The applications to infrared studies by the matrix isolation method are numerous and varied. The first applications were directed toward the spectra and structure elucidation of unstable free radicals. The free radicals may be prepared in the gas phase and quickly condensed along with a large amount of matrix material onto a cold surface. In this manner the infrared spectra of trichloromethyl and dichlorocarbene radicals have been studied[2,3]. Free radicals can also be generated in situ, by photolysis of a previously deposited reactant within an inert matrix. Thus, for example, the species HNO was produced by the photolysis of nitromethane in argon,[4] HCO has been produced by the photolysis of a mixture of HI and CO in an argon matrix,[5] HO_2 by the photolysis of HI or HBr and O_2 in argon,[6] etc. Reviews on the chemistry[7] and chemical physics[8,9] of matrix-isolated free radicals have been presented by Jacox and Milligan, and Pimentel. More recently Hallam[10] has tabulated every known free radical that has been studied by the matrix isolation technique. In this tabulation he also presents pertinent references and the methods of preparing these radicals within matrices. The use of matrix isolation in the study and characterization of high temperature species has been highly successful. Mass spectrometric methods have been used for the study of high temperature equilibria, but little structural information can be obtained by this method. The attainment of optical spectra of high temperature species in the gas phase is beset with experimental difficulties, such as the reaction of the hot gases with cell walls and windows, and the difficulty of attaining sufficient quantities of species of interest to allow spectral observations to be

made. Even when reproducible spectra can be observed, their interpretation is difficult because of the highly excited rotational and vibrational states involved. These difficulties can easily be overcome by simultaneously condensing along with the matrix gas the products formed by reaction in a Knudsen cell onto a cold surface. The spectra obtained from the resulting deposit consists of sharp bands whose analysis is much easier. By this technique the spectra and structures of alkaline earth dihalides[11], boron oxides[12], alkali-fluoride polymers[13] and many others have been examined.

The study of chemical reactions, photochemical reactions, and elucidation of likely mechanisms are other areas in which the matrix isolation method has proven of value. Two or more reactant molecules, each premixed with inert gas can be simultaneously deposited on a cold infrared window. The reaction can be easily controlled by warming the sample until diffusion takes place and reaction occurs. The reaction can be stopped at any convenient time or at specified intervals by recooling the sample. After recooling a spectral analysis of the products and/or reactants can be made. Similarly one can perform analysis of photolysis products as a function of time, the reaction being controlled by the turning on and off of the photolysis source.

For study of intermolecular interactions the matrix isolation technique is extremely valuable. By varying M/A ratios one can vary the degree of molecular association and interaction. The method finds extensive application in the study of hydrogen bonded species. Pimentel, et al.[14,15] studied the OH stretching region of water and methanol at various M/A ratios and were able to resolve the broad absorption observed in the pure sample in the OH stretching region, into components assign-

able to the monomer, dimer, trimer, etc., the spectral frequencies are usually very nearly equal to the gas phase frequencies. Further the bands are very sharp, affording better resolution of overlapping and broad bands. Hence the method is useful in obtaining vibrational assignments and frequencies for use in normal coordinate calculations.

As useful and valuable as the matrix isolation may be, it is not without its inherent problems. These problems vary from one experiment to the next and must be minimized as conditions allow. The thickness of the sample film, i.e., the number of absorbing molecules in the light path, is limited by the poor thermal conductance of the inner portion of the matrix film. Thus, the quality of the deposit decreases with film thickness and scattering of the incident light increases, resulting in poor spectra. Further the deposition rate affects the quality of the film. In general very slow deposition rates are desirable, but this depends somewhat on the heat of fusion of the gas and how fast this heat can be dissipated.

It is not clear or easily predictable to what extent the results depend on the matrix. In general the frequencies obtained are close to the gas phase values, but exceptions do occur. Further the mobility of species dispersed in matrices is difficult to assess. The efficiency of isolation of different matrix materials varies and the effects of multiple trapping sites can complicate spectra to some extent.

Raman Spectroscopy

In principle the data obtained from the Raman spectrum of a molecule in combination with the infrared data contain the frequencies of every optically active vibrational mode of the molecule. Depending on

the symmetry of the molecule the Raman spectrum may be the same as the infrared spectrum, or they may have some features in common, or in the case of centrosymmetric molecules, the two spectra will have no common features. Hence for most molecules the Raman spectrum is necessary for the complete assignment of vibrational frequencies. In the study of some systems the vibrational spectrum may not be conveniently accessible by infrared methods. The study of aqueous solutions is difficult to accomplish even when insoluble sample cell materials such as Irtran are available, due to the broad absorptions of water in the infrared region. Except for the OH stretching region the Raman spectrum is free of interferences. Also infrared techniques for low frequencies (0 - 250 cm^{-1}) are more complex whereas in Raman spectroscopy one can operate close to the exciting line with little difficulty. For making vibrational assignments, the polarization data available from the Raman spectrum is of considerable value. For totally symmetric vibrations the degree of depolarization of the Raman lines is between 0 and 6/7. With the usual sampling procedure the degree of polarization will be 6/7 for all other vibrations.

Until recently Raman spectroscopy had fallen into relative disuse because of its inherent experimental disadvantages relative to the infrared method. The magnitude of the intensity of Raman scattering is of the order of 10^{-5} times the intensity of the Rayleigh scattering which is in turn about 10^{-3} times the intensity of the exciting line. The unavailability of intense monochromatic light sources made the study of Raman spectra of dilute solutions, gases, and small sample volumes extremely difficult. Further the study of fluorescent or photosensitive compounds was nearly precluded when using the usual mercury discharge

light source. Even when sample requirements were optimum, the inherent difficulties of using the mercury discharge source, such as cooling, filtering of unwanted lines, etc., made Raman spectroscopy a tedious undertaking and highly impractical for routine analytical or commercial work.

The recent availability of low cost, dependable, and easy-to-operate laser sources has eliminated almost all of the sampling difficulties which once limited the use of Raman spectroscopy. The advantages of a laser source are numerous: 1) in commercially available systems a collimated beam of greater than 500 mw/mm^2 can be easily obtained so that transfer efficiency from source to sample can be high and very small sample volumes can be used; 2) such power densities can be confined to one laser line by use of modern filters and optical coatings; 3) the beam is coherent and polarized, making it a simple matter to obtain precise polarization measurements; 4) due to the extremely narrow linewidth of the laser lines greater resolution can be obtained; 5) with a wide choice of lasers and detectors available one can operate at almost any spectral region he desires so that fluorescent and absorbing samples are no longer a major problem; 6) the ease of handling and focusing a laser beam makes the use of many different sampling geometries available.

As a result of the recent surge of interest in Raman spectroscopy brought about by the introduction of laser sources, many advancements in the collection and detection of Raman scattering have occurred. Since the Raman spectrum is a set of weak emissions surrounding a highly intense exciting line, the monochromator must possess high discrimination. For good sensitivity the scattered and stray light intensity

level must be 10^{-8} times the source intensity at a distance of 10 Å from the exciting line. This performance is not available even with the best of single monochromators. For this reason a number of high quality double monochromators have been developed. Besides reducing stray light to a minimum these are also capable of higher resolution. Highly sensitive small area cathode photomultiplier tubes have been developed. By magnetic shielding and cooling of these tubes the background noise can be dramatically reduced. There are various techniques for amplifying the photomultiplier signal available. The usual direct current amplifier is successful for relatively large currents, but tends to be noisy and unreliable at low current levels. The photon counting method is highly successful at quite low signal levels, while at the same time requiring no changes in experimental design. Since the magnitude of the burst of electrons from the end of the dynode chain should be about the same for each individual photon, with proper blocking circuitry it should be possible to pick out of the array of pulses only those which originate from single photon events at the photocathode. Most of the noise pulses will be larger or smaller than photon pulses. So by setting an upper and lower limit on the pulse height the background noise can be effectively eliminated. The use of lock-in amplifiers has also been successful for improving signal-to-noise ratios. By this method, the beam is chopped at a frequency of several hundred cycles-per-second. Only those signals which arrive in-phase with the chopping waveform are amplified. Thus random noise is effectively discriminated against. However, in neither of these methods is scattered light or grating ghosts eliminated.

Raman Spectrum of Matrix-Isolated Species

From the discussion of the matrix isolation method, it is easy to see that the complimentary data from the Raman spectrum of these systems would be of significant value. The nature of many free radical systems can be considerably different from structurally similar stable compounds. Hence assignment of infrared data based on analogous stable compounds can be uncertain. Certainly the assignment of vibrational data rests on surer footing if the Raman spectrum is known. Further the low frequency region (0 - 250 cm^{-1}) is more easily studied by Raman spectroscopy. If polarization measurements can be made on matrix isolated species, this information would be of immense value.

The difficulties in the infrared studies of matrix isolated species can only be expected to be multiplied in the corresponding Raman study. The inherent weakness of the Raman effect precluded the study of matrix isolated species entirely before the laser sources were made available. Even with these powerful light sources, the dilution of the sample by two or three orders of magnitude makes the Raman study by matrix isolation a difficult task. Hence the Raman scattering must be maximized by good experimental design, while the background noise and scattering must be brought to an absolute minimum.

Since the laser beam can be collimated to the extent that divergence is negligible over a long distance there are several ways of building multireflection sampling cells such that one can maximize the amount of Raman scattering obtained. It has been demonstrated here and elsewhere[16] that very good Raman spectra can be obtained with a single reflection from a thin film. In principle many reflections should result in much stronger scattering, although this has not been found to be

true in preliminary efforts.

Having designed suitable sampling devices such that the Raman scattering is maximized, there remains to be optimized the signal-to-noise ratio. The problem of scattering and grating ghosts can be somewhat alleviated by the use of an interference filter between sample and monochromator which will block the exciting wavelength but pass the Raman emissions. With modern optical coatings this can be done quite efficiently. An ingenious technique using lock-in amplification and a chopper devised from a spike reflection filter and a neutral density filter has been recently described.[17] By this technique the Raman spectrum is chopped and phase detected while the Rayleigh scattering, unwanted scattered light, and grating ghosts are not. Hence by this method both random background noise and stray light can both be eliminated.

The Nitrates

The nitrate ion, particularly in the form of alkali-metal nitrates, has been thoroughly studied in the solid phase, melt phase, and in aqueous solution. The infrared and Raman spectra of the ordered crystalline phase are fairly well understood. However, the spectral features of the melts, concentrated solutions, and disordered solids have led to differing opinions regarding the detailed nature of the ionic interactions involved.

The unperturbed nitrate ion has a planar trigonal structure and belongs to the D_{3h} symmetry point group. The symmetry classifications, selection rules, and frequencies[18] for the ion in dilute aqueous solution are presented in Table I.

TABLE I

UNPERTURBED NITRATE SELECTION RULES

Mode	Symmetry	Activity	Frequency cm^{-1}	Description
ν_1	A_1'	R, p	1050	symmetric NO stretch
ν_2	A_2''	IR	820	out of plane bend
ν_3	E'	IR, R, dp	1390	asymmetric NO stretch
ν_4	E'	IR, R, dp	720	planar bend

Any deviations from these selection rules, splitting of the degenerate modes, or shifts in these frequencies, can be interpreted in terms of the symmetry and strength of the forces perturbing the ion. Hence the vibrational spectrum of the ion is a sensitive probe of the ionic environment. Numerous studies have been made on aqueous metal-nitrate solutions.[19,20,21] In dilute solutions (< 1 N.) the selection rules given in Table I are approximately obeyed, and the frequencies listed therein are obtained. The only difference noted from this table is in the behavior of ν_3. Even in very dilute solutions ν_3 is split by ca. 56 cm^{-1}.[21] This splitting is observed in all dilute metal nitrate solutions, and presumably results from a distortion of the nitrate ion by some well-defined solvation sphere about the ion.

In more concentrated solutions band positions, intensities, and half-widths show a marked concentration and cation dependence. These changes in spectral features have been interpreted in terms of various interactions of solvated ions, ranging from discrete contact-ion pairs,[22]

solvent-separated ion pairs, or short-range order approaching that of the hydrated crystals.[19]

A considerable amount of research activity in recent years has been directed toward the study of the vibrational spectra of molten salt systems. Because they have relatively low melting points, a wide liquid phase temperature range, and are stable toward decomposition, the nitrates have been the focus of most of these studies, particularly the alkali-metal nitrates.

As with the aqueous solutions, the detailed nature of the ionic interactions in the melt phase is still not clearly understood. The vibrational spectra of univalent nitrates show a number of interesting changes upon melting. Among these may be enumerated: 1) the loss of degeneracy of ν_3 and ν_4, in some cases; 2) the appearance of frequencies in both the infrared and Raman spectra which are forbidden by the D_{3h} selection rules listed in Table I; 3) a regular change in ν_1 as the cationic species is changed; 4) and, the appearance of low-frequency bands in the infrared spectra.

To account for these spectral features a number of models of the molten state have emerged. Wait, Ward, and Janz[23] assumed that the melt phase was predominantly anion-cation contact pairs so that the nitrate ion symmetry was lowered to C_{2v} or C_s by a unidentate attachment of the metal to a nitrate oxygen. Using data from the literature they assigned vibrational frequencies on the basis of a C_{2v} model and calculated Urey-Bradley force constants for the alkali-metal nitrates, silver nitrate, and thallous nitrate. These force constants were then related to the magnitude of the pairwise interactions. Further discussion of this model and some pertinent calculations are included in Chapter IV.

An interesting interpretation of the splitting of ν_3 has been proposed by Chisler.[24] Citing the ν_3 splitting observed in dilute solution, which is independent of concentration, cation type, and temperature, he proposed that the free nitrate ion is distorted, via the Jahn-Teller effect, to a planar group having a symmetry lower than D_{3h}. To support this conclusion he presented a qualitative molecular orbital description of the NO_3^- energy levels. In this approximation he demonstrated the possibility of a degenerate ground state electronic configuration for the nitrate ion. This is a necessary condition for Jahn-Teller instability. However, his calculation is very qualitative, and his assumptions unfounded. Further the Jahn-Teller effect on s and p orbitals is not expected to be significant. Finally any such distortions would be expected to show up in the electronic spectrum. The electronic spectrum[25] is in agreement with currently accepted views[26] of the electronic structure of NO_3^-, which place the ground state in an A_1' configuration, i.e., nondegenerate.

In a number of more recent studies, various authors have concluded that the nitrate melt systems are characterized by a significant degree of order. Devlin, Williamson, and Li[27] used attenuated-total-reflection infrared spectroscopy and thin-film transmission techniques to obtain relatively high resolution data on the melts of lithium, sodium, and potassium nitrates. Their studies revealed a number of previously unobserved features in the nitrate melt spectrum. Their data when combined with published Raman data[28] showed multiplet structure even for the nondegenerate modes ν_1 and ν_2. Convinced that the splitting of the NO_3^- internal vibrations resulted from a combination of site effects and correlation field effects, they proposed a perturbed lattice struc-

ture. Noting that their data was consistent with an orthorhombic lattice similar to the room temperature form of KNO_3, they made assignments based on a perturbed orthorbombic lattice model.

In a detailed Raman study of molten $LiNO_3$, $NaNO_3$, and $AgNO_3$, James and Leong[29] also concluded that the melt systems were best described by a model involving quasicrystalline units. However, they argued that the crystallites produced by an orthorhombic packing would be incompatible with the kinetic freedom of the melts. By analogy with the structural changes observed upon heating $RbNO_3$ through its phase changes, they proposed a cubic lattice structure. Applying this model to $LiNO_3$ and $NaNO_3$ they successfully rationalized the spectral variations, volume change on fusion, entropies of fusion, and radial distribution functions for the melt. However, this model was not adequate to describe the behavior of $AgNO_3$.

In both the orthorhombic model and the quasicubic model, a center of symmetry is implied. This was supported by an apparent lack of coincidence between Raman and infrared frequencies. However, the infrared frequencies were obtained from a decomposition of broad ATR curves into component bands. It has been shown recently[30] that this is not a valid procedure, at least for the solid state spectra. It is now recognized that the peak in the solid state ATR TM wave curves corresponds to the transverse optical (TO) phonon interaction while the inflection point on the high frequency wing corresponds to the longitudinal optical (LO) phonon.

For nitrates with no center of symmetry, e.g., trigonal ordered KNO_3(III), the Raman components coincide closely with TO and LO valves deduced from the TM ATR curve[31]. Impressed by similar observations on

the nitrate melt systems, Devlin, et al, proposed that the ν_3 splitting may not be due to distortion splitting or correlation field splitting, but rather to TO-LO splitting. This implies that the melt systems have sufficient short range order to support optical phonons and further that the structural units must be similar to the corresponding solids. The similarity is evidenced by the rather nondramatic changes in the spectra at the point of fusion. However, the presence of TO and LO features in the Raman spectrum obviously precludes any center of symmetry, so that by this model interpretations based on centrosymmetric models of the quasicrystalline state are invalidated.

In summary we may conclude that the quasicrystalline nature of the melt systems is fairly well established. The specific "lattice" type is not well established, and it is not likely that any particular geometry will describe all nitrates. It can also be seen that there is no justification for the widely used practice of deciding on the presence of ion pairs or ion complexes by the application of symmetry selection rules for the isolated molecules or complexes. Any selection rules must be based on the proposed symmetry of the liquid structure in a manner analogous to the deduction of solid state selection rules based on the crystalline space group.

Now in the present investigation the nitrates will be studied in monomeric form. The spectra will hence be free from any significant intermolecular, i.e., correlation field splittings, TO-LO splittings, and nearest neighbor site splittings. Under these conditions the nitrate ion should experience the maximum amount of distortion possible by cationic electrostatic interaction in that each anion will be strongly associated with only one cation, rather than situated on a site in a

cation shell. The nature and magnitude of this distortion will be deduced from the changes in the vibrational spectra, particularly in the ν_3 region. From these results it should be possible to make more quantitative estimates of anionic distortion in nitrate melt and solution systems and, in particular, to construct further arguments as to the reasonableness of attributing certain splittings to anion distortion. It is of interest to note that no matrix-isolation infrared studies have been made on high temperature species containing polyatomic ions.

CHAPTER II

EXPERIMENTAL

The Cell

The experimental phase of this study consisted of isolating the various nitrates in monomeric form in such a manner that their infrared and Raman spectra could be obtained. The requirements for successful matrix isolation, portability, and simultaneous infrared and Raman sampling capability, impose several restrictions on permissable cell designs. The cell must be able to maintain a moderate vacuum (ca. 10^{-5} torr) for several hours. Heat leaks must be minimized to economize on refrigerant use and to avoid frequent refrigerant refillings. The physical dimensions of the cell must be within the limitations of both the infrared and Raman sampling compartments. Finally, the cell must be reasonably robust and portable.

A diagram of the cell and associated apparatus is shown in Figure 1. The outer wall (A) and nitrogen compartment (B) were constructed of standard type 304 schedule 5 welded stainless steel pipe. To the bottom of the nitrogen compartment was attached a removable polished copper radiation shield (C) which extended below and surrounded the sampling block (D). The silvered pyrex inner dewar (E) and copper sampling block were suspended, via a Kovar-to-glass seal, from a rotatable tapered joint, so that the sampling block could be faced toward either the outer windows (F) or the vacuum ports (see Figure 2). The bottom of the cell

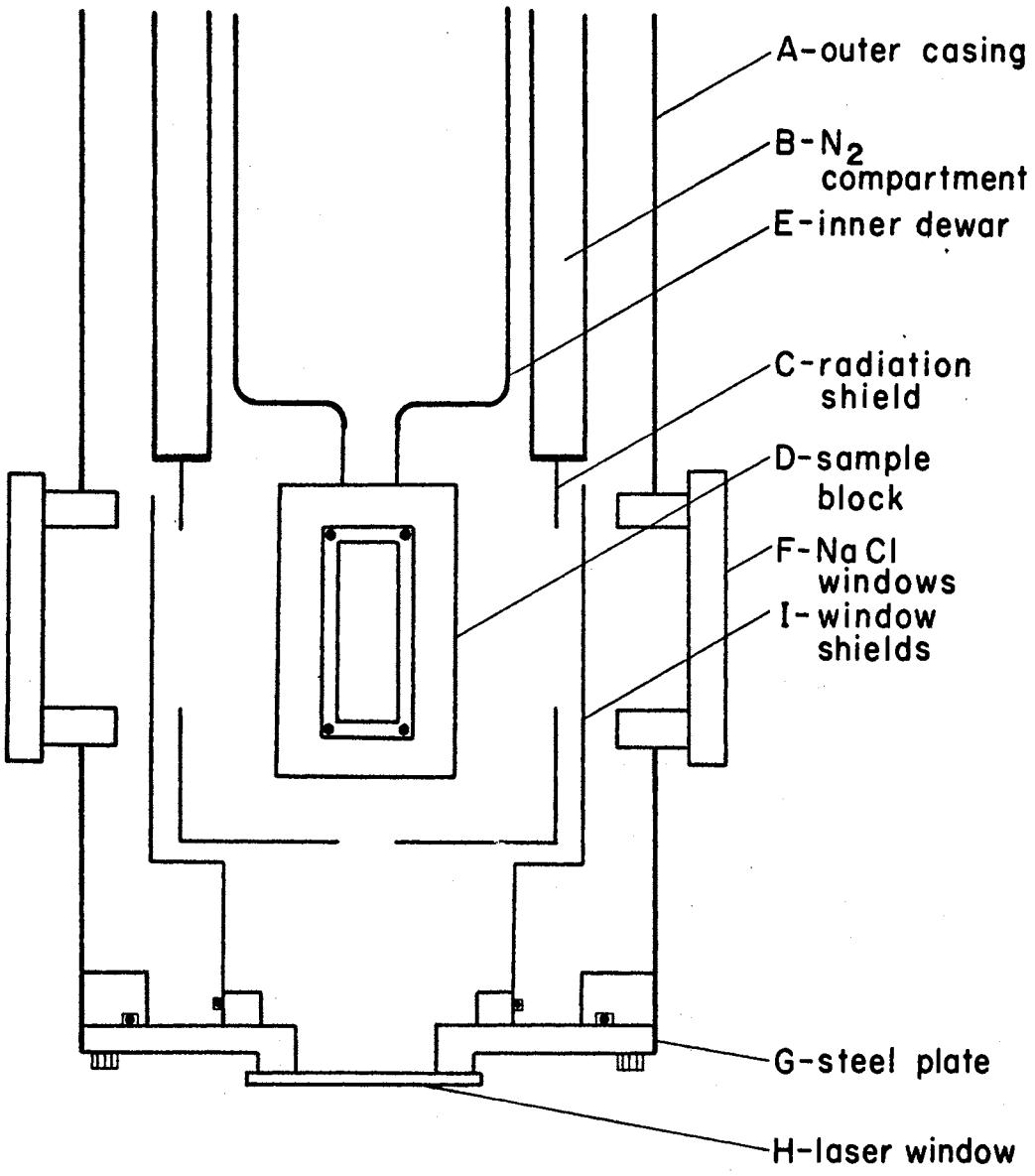

Figure 1. Cutaway View of Matrix-Isolation Dewar

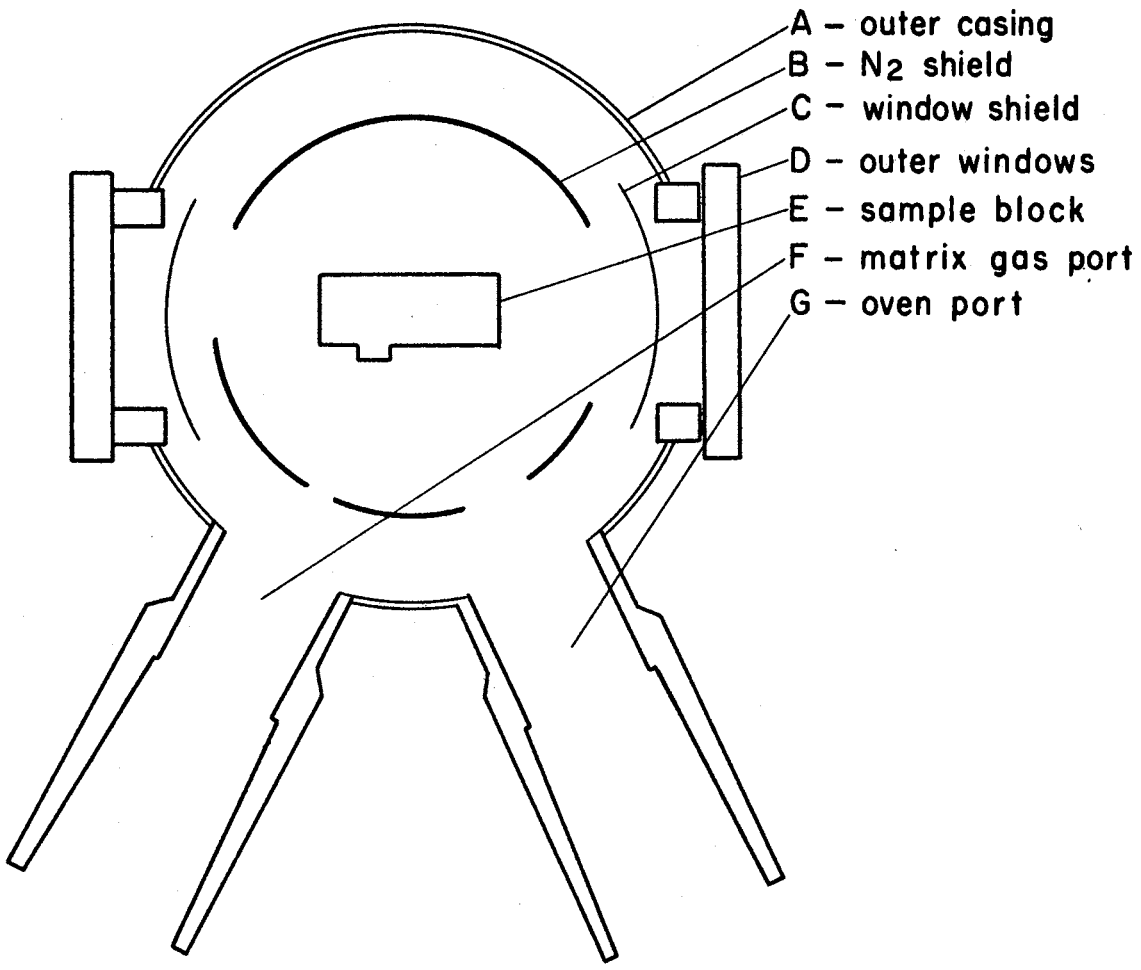

Figure 2. View From Bottom of Cell Showing Relationship of Sample Block, Shields, and Outer Windows

was a steel plate (G) attached with a rotatable O-ring seal. To this plate was attached a glass window (H) for the passage of the laser beam through the bottom of the cell. Also attached to this plate was a pair of aluminum shields (I) which protected the inner surfaces of the outer windows during deposition. After sample deposition the bottom plate was rotated 60° to remove these shields from the light path.

The copper sample block was hollow so that the refrigerant could circulate on all four sides of the deposition window (see Figure 3). The sodium chloride deposition window was mounted against a shoulder inside a rectangular hole in the block, and kept in place by a copper frame screwed to the block. Good thermal contact was achieved by the use of indium wire gaskets between these elements. The temperature was recorded by a copper-constantan thermocouple inserted into a .030" hole drilled into the window.

Raman scattering was obtained from a single reflection of the laser beam off the face of a polished aluminum wedge affixed to the copper sample block in such a manner that the laser beam incidence angle was 10°. By using this arrangement the samples for both the infrared and Raman investigations could be deposited simultaneously. The two sodium chloride windows for transmission of the infrared beam and collection of the Raman signals were attached with Apiezon T vacuum grease to stainless steel flanges welded to the outer casing of the dewar.

The nitrates were deposited from a stainless steel Knudsen cell contained in a quartz tube which was heated by a coil of No. 24 chromel A resistance wire. The quartz tube was supported by a nylon plug which fit inside the bore of a 29/42 standard taper O-ring joint (see Figure 4). The temperature was measured by an iron-constantan thermocouple in

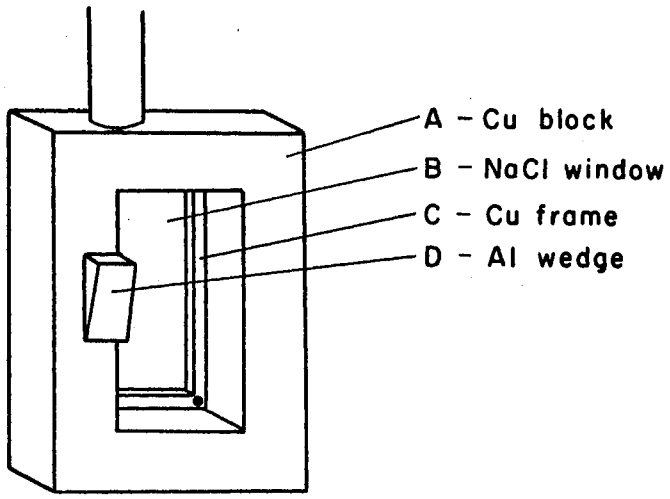

Figure 3. Sample Block

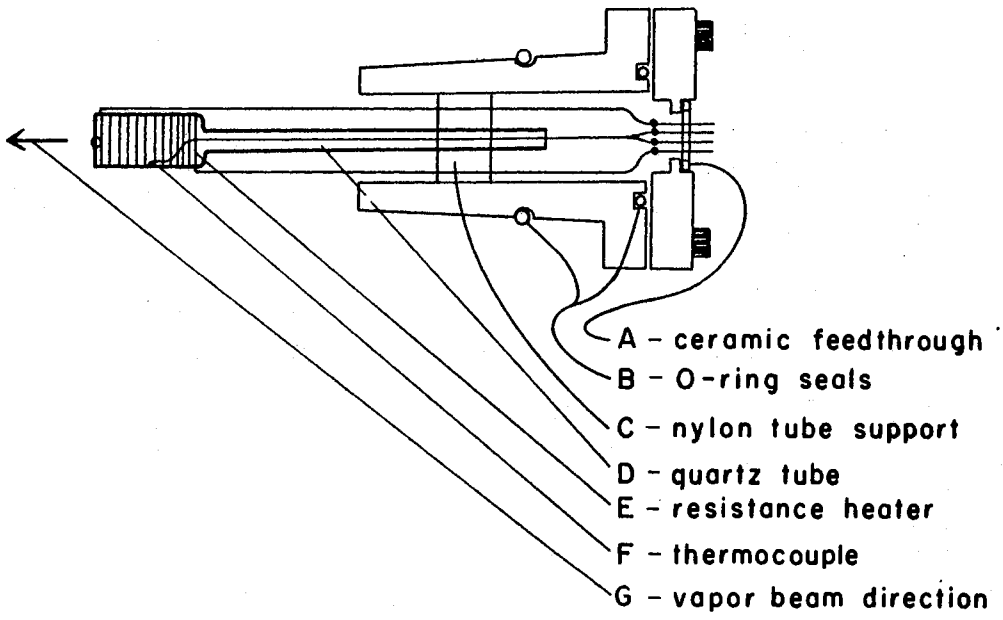

Figure 4. Oven Assembly

contact with the Knudsen cell. The whole oven assembly was mounted in a matching 29/42 standard taper joint welded to the outer casing of the dewar in such a manner that the beam of particles was directed toward the deposition window.

The matrix gas was passed into the cell from a portal adjacent to the oven. The flow rate was estimated by means of a Fischer and Porter variable area flow meter.

A rough calculation of the major heat leaks,[32] i.e., conduction of heat down the walls of the neck of the central dewar, radiation from the nitrogen shield, and conduction through the residual gas indicated an approximate heat input to the helium dewar of about 0.15 watt. This would indicate a filling of liquid helium should last about two hours. With the oven and matrix gas off this loss rate was achieved. However, during deposition the boil-off rate was substantially higher. Although this refrigerant capacity is rather small, it was felt that the convenience of a small, rather portable cell outweighed the inconvenience of refilling once or twice during an experiment. Further, a considerable amount of work was done at liquid nitrogen temperature, in which case a filling with no shielding lasted about 30 hours, or with shielding, about 5 days. Helium was transferred into the dewar with an Andonian Associates standard helium transfer line.

Procedure

The typical experimental procedure was as follows. The Knudsen cell and oven assembly were loaded in a nitrogen purged glove bag. The oven assembly was then installed in the cell and the cell was pumped for several hours to a pressure of ca. 10^{-6} torr. The nitrogen shield

was filled and the inner dewar precooled with liquid nitrogen. After precooling the transfer tube was inserted and sufficient liquid helium was transferred to cool down the cell and collect a small amount of liquid in the bottom of the dewar. The liquid flow rate was then reduced to the point necessary only to maintain this volume of liquid during the deposition period. The matrix gas was then started at a flow rate of ca. 10^{-3} moles/min, and the oven was turned on. Oven temperatures were ca. 110° for $Cu(NO_3)_2$ and ca. 400° for the alkali-metal nitrates. During deposition the pressure was ca. 10^{-5} torr. After the deposition, which usually lasted about an hour, the helium dewar was filled and the cell was removed from the vacuum line for spectroscopic observations.

When CO_2 or CCl_4 was used for the matrix material, the inner dewar was filled with liquid nitrogen. The deposition procedure was the same except that no refrigerant refillings were necessary.

Preparation of Compounds

The alkali-metal nitrates were reagent grade anhydrous salts. These were recrystallized from triply distilled water and dried under vacuum.

Anhydrous cupric nitrate cannot be prepared in such a simple manner, as the water of hydration is rather strongly bound. Any attempts to dry this by ordinary methods produces nonvolatile oxides or oxonitrates. Hence the compound must be prepared under anhydrous conditions.

Anhydrous cupric nitrate was prepared by reaction of copper metal with a solution of dinitrogen tetroxide in ethyl acetate. The procedure was similar to that described by Addison and Hathaway.[33] About 10 ml.

of Fisher reagent grade ethyl acetate was dried over activated alumina and added to 10 ml. of vacuum distilled N_2O_4. To this was added 2 grams of Cu foil. The vigorous reaction was allowed to proceed to completion in a flask provided with a pressure relief device to bleed off the evolved nitric oxide. The flask was then attached to the vacuum line and the excess N_2O_4 and ethylacetate were pumped off. This left a green amorphous solid which was then purified by sublimation at ca. 150° C. The resulting deep blue vrystals were then transferred to Knudsen cells in a drybox and stored in a dessicator.

Instrumentation

All infrared spectra were recorded on a Beckman IR-7 infrared spectrophotometer. Standard NaCl and CsI optics were used to scan the infrared spectrum from 250 cm^{-1} to 4000 cm^{-1}.

The Raman apparatus was an assemblage of various commercial components chosen on the basis of their compatability, reputed reliability and cost. The monochromator was equipped with a cooled FW-130 photomultiplier tube. The monochromator was actually a pair of one-meter Czerny-Turner monochromators mechanically coupled in such a manner as to bring stray light levels down to a minimum. The FW-130 photomultiplier tube has a small slit-shaped cathode as compared to conventional tubes which have a relatively large circular cathode. This tube, when cooled and properly aligned, produces much less background noise than the conventional tubes (ca. 2 thermal emissions/sec).

Initially two separate detection systems were provided. For large signals, a Kiethley 417 High Speed Picoammeter was used to amplify the photomultiplier tube current directly. For weaker signals a Hamner

photon counting system was provided. Because of its ability to discriminate against photomultiplier pulses of improper magnitude, i.e., those which originate from sources other than the primary cathode, the photon counting system provides high signal-to-noise ratio. In practice it was found that the photon counting system was superior for both large and small signal levels, and hence the DC amplification method was abandoned.

The Raman excitation sources were a Spectra-Physics Model 125 helium-neon laser and a Coherent Radiation Laboratories Model 52 argon ion laser. The helium-neon laser had a power output of ca. 50 milliwatt at 6328 Å. The argon ion laser was tunable and provided ca. 1000 milliwatts at 4880 Å and 5145 Å. Lesser amounts of power were available in several other lines. The lasers were placed in convenient positions and their beams deflected by appropriate lens and mirror systems to an optical bench situated near the entrance slit of the monochromator, as shown in Figure 5. The Raman scattered photons were collected by an Auto Mamiya Sekor F 1.8 camera lens and focused onto the entrance slit. The optical bench and associated optics were enclosed in a light-tight enclosure.

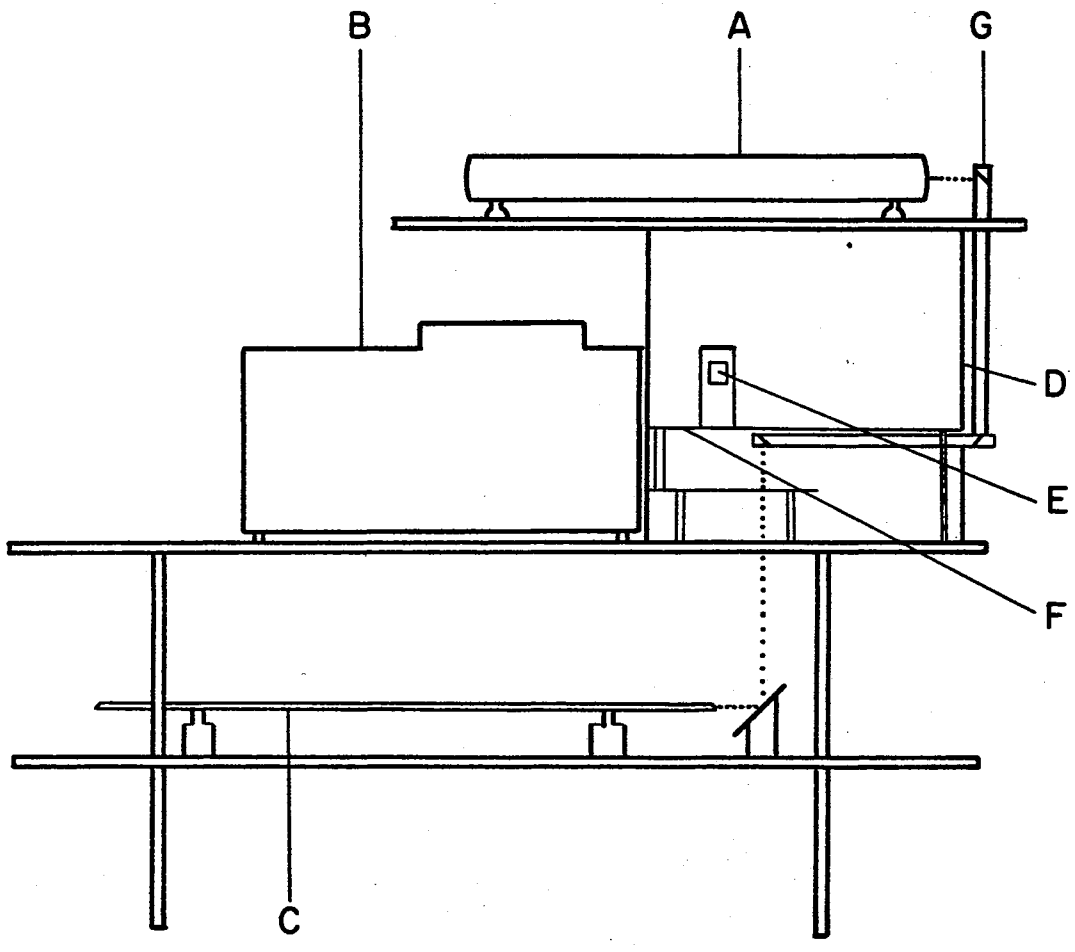

A – argon ion laser
B – monochromator
C – He-Ne laser
D – enclosure
E – collection lens
F – optical bench
G – beam transfer optics

Figure 5. Schematic of Raman Apparatus

CHAPTER III

RESULTS

As mentioned in the introductory chapter, one of the goals of this project was the development of techniques and apparatus for the investigation of Raman spectra of thin films. Before presenting the nitrate results, the results of a few preliminary investigations will be presented to draw attention to the limitations of this technique.

Shown in Figure 6 is the Raman spectrum of a thin film of CCl_4. This molecule was chosen because it is known to have intense Raman lines, and because the isotbpic splitting of ν_1 (the symmetric stretching mode) offers a striking demonstration of the resolving power of the instrument. The ^{35}Cl-^{37}Cl isotopic splitting is shown in Figure 7.

As mentioned, CCl_4 is known to have a very intense Raman spectrum. Hence the spectra in Figures 6 and 7 are somewhat misleading. The spectra were obtained under moderate sensitivity, and the sample film was several times the thickness necessary for infrared studies. In Figure 8 is the Raman spectrum of CCl_4 in a matrix of CO_2. The ratio CO_2:CCl_4 is 100:1, and the thickness is at a maximum. This maximum thickness is imposed by the thermal conductivity of the film. There is no difference in the peak positions, relative to pure CCl_4 film, of course, but the detector sensitivity is two orders of magnitude higher, nearly the upper limit of instrumental sensitivity. A portion of the infrared spectrum of this same sample is shown in Figure 9. From this

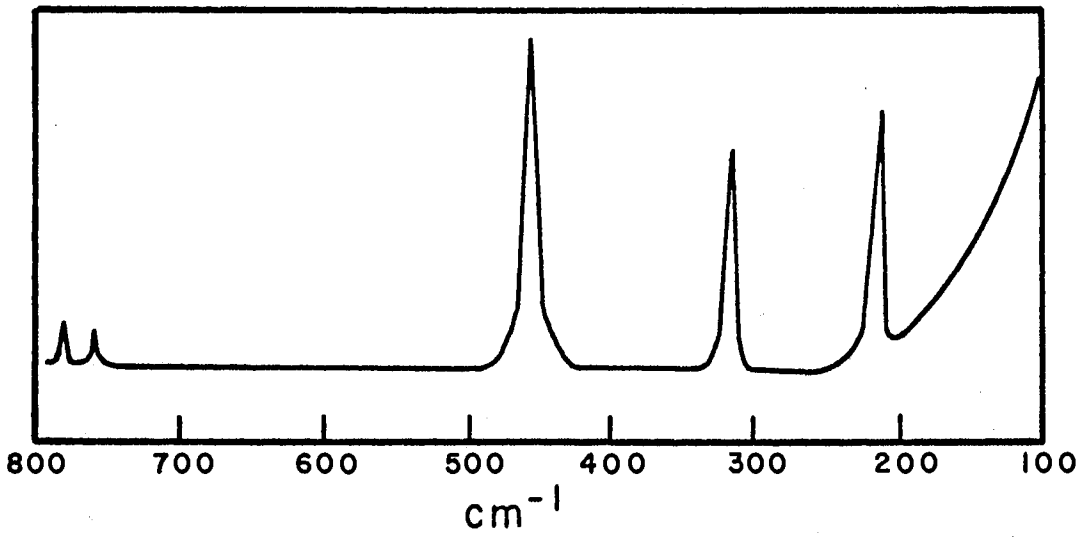

Figure 6. Raman Spectrum of a Thin Film of CCl_4 at 77°K

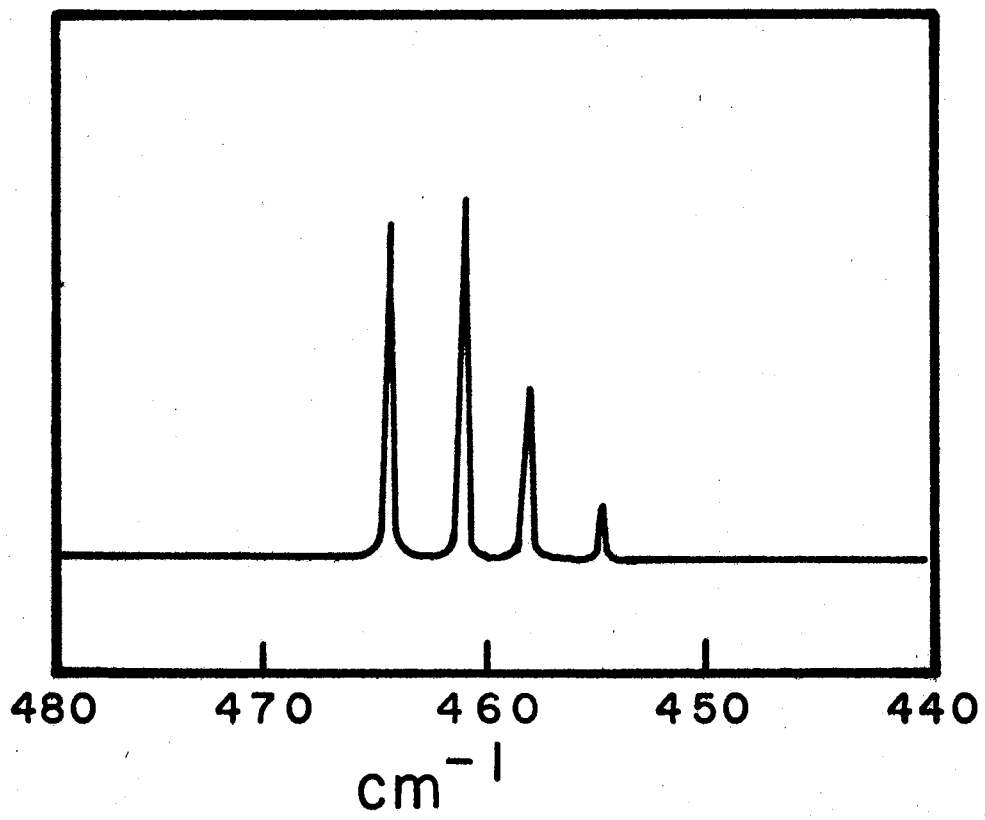

Figure 7. High Resolution Scan of 460 cm^{-1} Line of CCl_4. Same Sample as in Figure 6

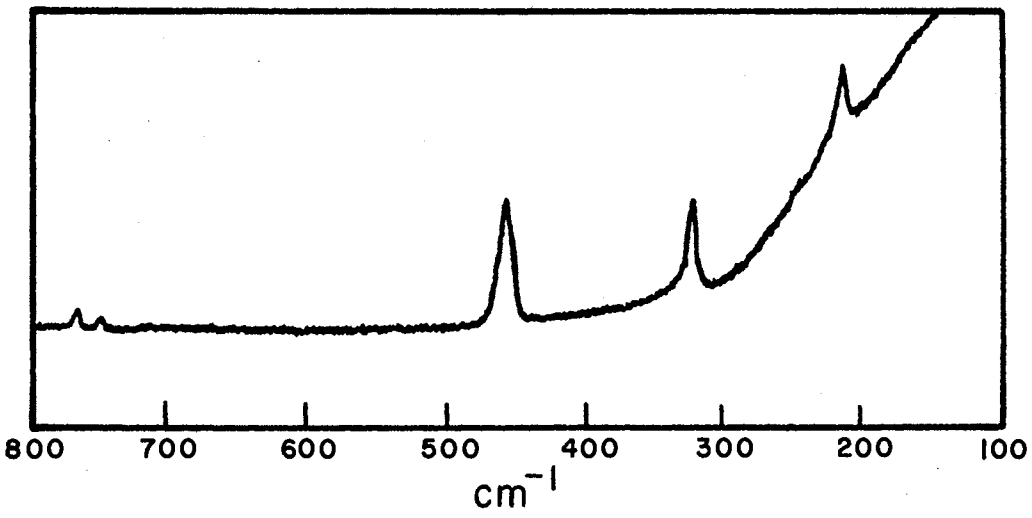

Figure 8. Raman Spectrum of CCl_4 Diluted 100:1 in CO_2 Matrix. Background Removed

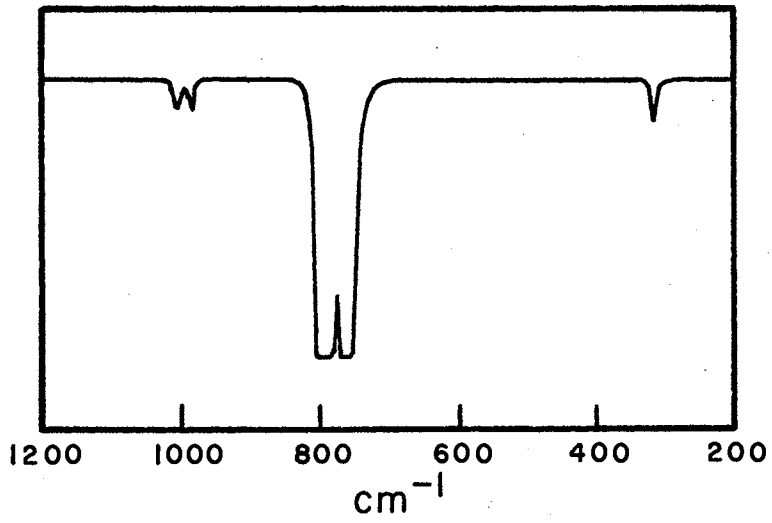

Figure 9. Infrared Spectrum of CCl_4 Diluted 100:1 in CO_2 Matrix

it can be seen that the film is still about twice as thick (or twice as concentrated) as that required for normal infrared sampling. Now, since in most cases a M:A ratio of at least 500:1 is required for good isolation, it is obvious that only those molecules expected to have an intense Raman spectrum can be studied in this manner. Further the film thickness must be two to three times that required for normal infrared investigations.

For the nitrate systems, ν_1 is invariably several times more intense than the other Raman active vibrations. Hence for the isolated nitrate monomers, we should not be surprised if ν_1 (or its analog in the resulting monomeric geometry) is the only detectable vibrational mode in the Raman spectrum.

For the alkali-metal nitrates a series of matrix isolation experiments were performed in matrices of Ar, CO_2, and CCl_4. It is well known [13] that the frequencies observed are somewhat dependent on the particular matrix material used. Hence the different matrix materials were used in order to insure against making conclusions based on what could possibly be spurious matrix effects. Further, CCl_4 and CO_2 form rigid matrices at liquid nitrogen temperature. Although these compounds have a strong background spectrum of their own, their use affords a considerable economy over matrix materials such as argon, which necessitates the use of liquid helium.

The infrared spectrum of KNO_3 isolated in an argon matrix is shown in Figure 10. For comparison an infrared spectrum of a thin film of pure KNO_3 is shown in Figure 11. The most notable changes are the splitting of ν_3 and the 20 cm^{-1} red shift of ν_1. The broad ν_3 band in the solid is replaced by two distinct pairs of narrow bands in the

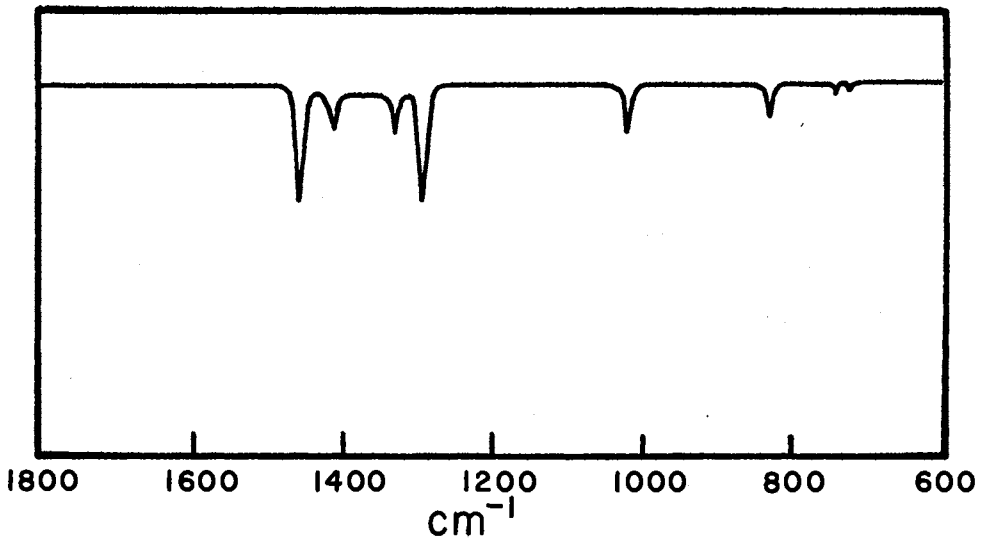

Figure 10. Infrared Spectrum of KNO_3 Isolated in Ar

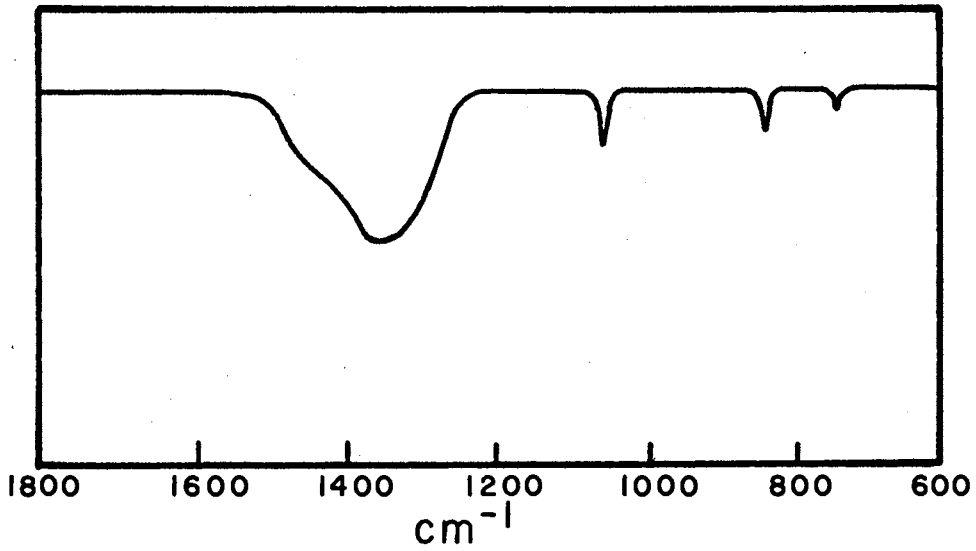

Figure 11. Infrared Spectrum of a Thin Film of KNO_3

isolated molecule spectrum. Further by changing the M/A ratio, the relative intensities of the 1291-1462 cm^{-1} pair and the 1334-1417 cm^{-1} pair can be altered. At high dilution the 1291-1462 cm^{-1} pair dominate over the 1334-1417 cm^{-1} pair. From these observations it was concluded that the 1291-1462 cm^{-1} pair were the distortion-split components of ν_3 for the monomeric KNO_3. The 1334-1417 cm^{-1} pair evidently belong to a polymeric species, probably a dimer. The presence of dimers in the vapors of alkali halides has been established by mass spectroscopic studies[50] and was later confirmed by matrix isolation studies.[51] Hence it is not unexpected that dimeric species should occur in the vapors of alkali-metal nitrates. Further support for this proposed assignment is shown in Figure 12. This shows the spectrum of 95% ^{15}N enriched KNO_3 and a 50-50 mixture of $K^{15}NO_3$ and $K^{14}NO_3$.

For a 50-50 mixture of $K^{14}NO_3$ and $K^{15}NO_3$, we would expect the monomer bands to appear at approximately equal intensity, with a ca. 30 cm^{-1} red shift for the ^{15}N monomer. The mixed ^{14}N-^{15}N dimer should predominate, but the intensity ratios are difficult to estimate because the dimer bands must split more or less depending on the strength of the interaction between the two nitrates. As can be seen the two strong peaks at 1291 cm^{-1} and 1462 cm^{-1} are accompanied by another pair of intense peaks at 1265 cm^{-1} and 1435 cm^{-1} respectively and show no splitting indicating that these are monomer bands. Likewise, the bands for the $^{14}N^{14}N$ and $^{15}N^{15}N$ dimers are apparent but it is difficult to assign the other weak features.

As expected the Raman spectrum of the isolated species is indeed weak. This is demonstrated in Figure 13. The instrument sensitivity is at an absolute maximum, and the only observable peaks are at 1036

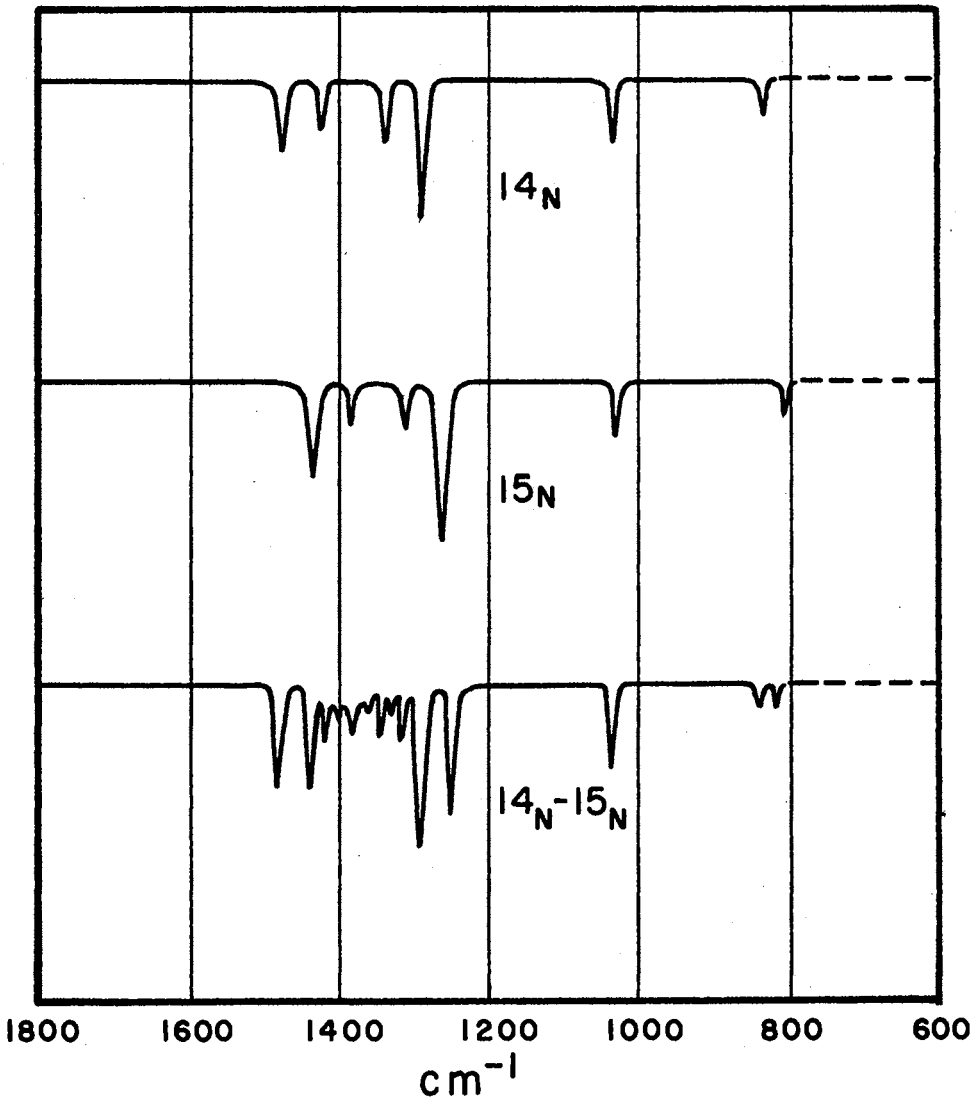

Figure 12. Infrared Spectra of Matrix-Isolated KNO_3, $K^{15}NO_3$, and 50% ^{15}N Enriched KNO_3

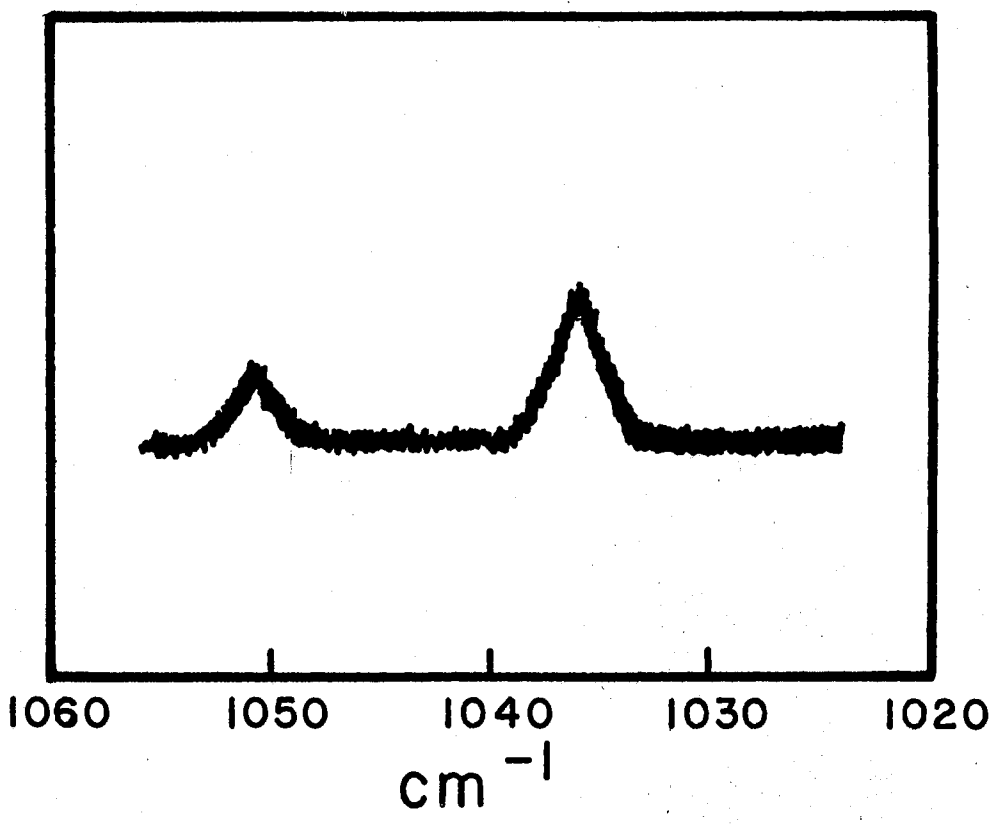

Figure 13. Raman Spectrum of 1050 cm^{-1} Region of Matrix-Isolated KNO_3

cm^{-1} and 1051 cm^{-1}. The 1036 cm^{-1} Raman line is in good agreement with the 1035 cm^{-1} infrared band. However, in the infrared spectrum ν_1 for the dimer is observed at 1047 cm^{-1}. The presence of a line in the Raman spectrum at 1051 cm^{-1}, and no line at 1047 may be indicative of a center of symmetry in the dimer. Further evidence for this conclusion resides in the fact that no splitting is observed in the infrared spectrum of the dimer. The strength of the interaction necessary to allow a stable dimer in the gas phase should be sufficient to cause a splitting of the components of ν_3. If a center of symmetry is present these components will be split in such a manner that one mode will be infrared active and the other Raman active. The same argument holds true for all the other modes, i.e., ν_1, ν_2, and ν_4 should be split also. As mentioned ν_1 is split, based on the infrared and Raman comparison, but the splitting is only a few wavenumbers indicating only a small degree of coupling, i.e., a weak interaction.

A possible structure for the dimer consistent with these observations is shown in Figure 14. Depending on whether or not this structure is planar, it would have C_{2h} or C_i symmetry. In either case each vibrational mode in the monomer would split into two modes, one Raman active and one infrared active, upon formation of the dimer.

There were no major differences between the spectra of KNO_3 isolated in Ar, CO_2 and CCl_4. In Figure 15 is shown the ν_3 region for the isolated monomer. In all three cases the splitting of ν_3 is about the same. However, the intensity of the high frequency component and the positions of the individual peaks are seen to depend on the matrix. Also there appears a small amount of splitting of the peaks in Ar and CO_2 which is not present in CCl_4.

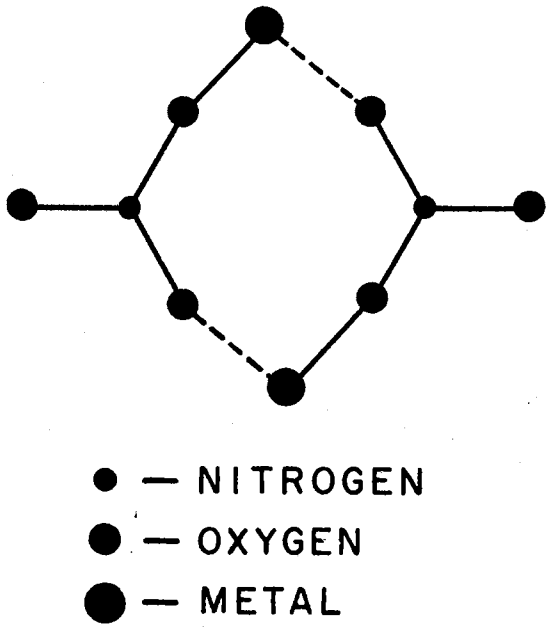

Figure 14. Tentative Structure for the Alkali-Metal Nitrate Dimer

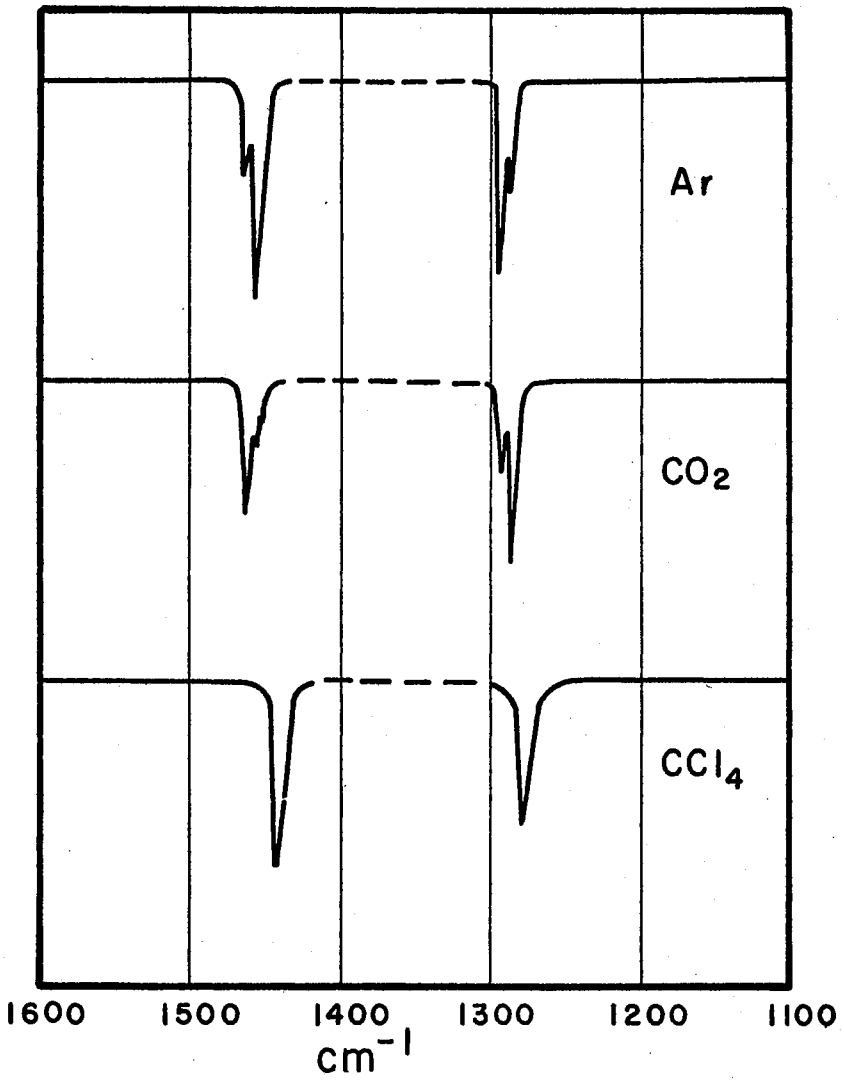

Figure 15. ν_3 Region of Infrared Spectra of KNO_3 Isolated in Ar, CO_2, and CCl_4

The region 200 cm^{-1} to 600 cm^{-1} was investigated with the hope of seeing the metal-oxygen stretching vibration which would be expected to appear at ca. 200-400 cm^{-1}. No such mode was found, indicating it either is below 200 cm^{-1} (the lower frequency limit of the instrument) or it is weak relative to ν_1 or ν_2, and thus not observable with the infrared instrumentation used. That the latter is probable was indicated by the fact that no distinct bands were found upon investigation of a thick sample (ca. 200μ) of $LiNO_3$ on a silicon platelet. Using a higher quality far-infrared instrument Ferraro and Walker[34] report a strong band at 321 cm^{-1} for $LiNO_3$ dispersed in a Nujol mull. Hence with the available infrared instrumentation, it is not surprising that the monomer metal-oxygen stretching mode is not observable. Since this region is close to the exciting line in the Raman spectrum, the signal-to-noise ratio is low and, therefore, this vibration would be even more difficult to detect in the Raman spectrum.

The planar bending mode ν_4 is also known to be weak in the infrared spectrum, relative to ν_2. It did appear in the KNO_3 spectrum, but only as a pair of very weak bands. It was not observed at all for the other alkali-metal nitrates.

The discussion thus far has been centered on KNO_3, since the major features are the same for all of the alkali-metal nitrates. The spectra for the rest of the alkali-metal nitrates are shown in Figure 16. These results are tabulated in Table II. The major trends apparent from this table are: (1) a regular increase in ν_1: (2) a regular decrease in the splitting of ν_3; and; (3) a very slight change in ν_2 in going from $NaNO_3$ to $RbNO_3$. Table III shows the results for varying matrix materials. Although admittedly sketchy, the results clearly indicate that only

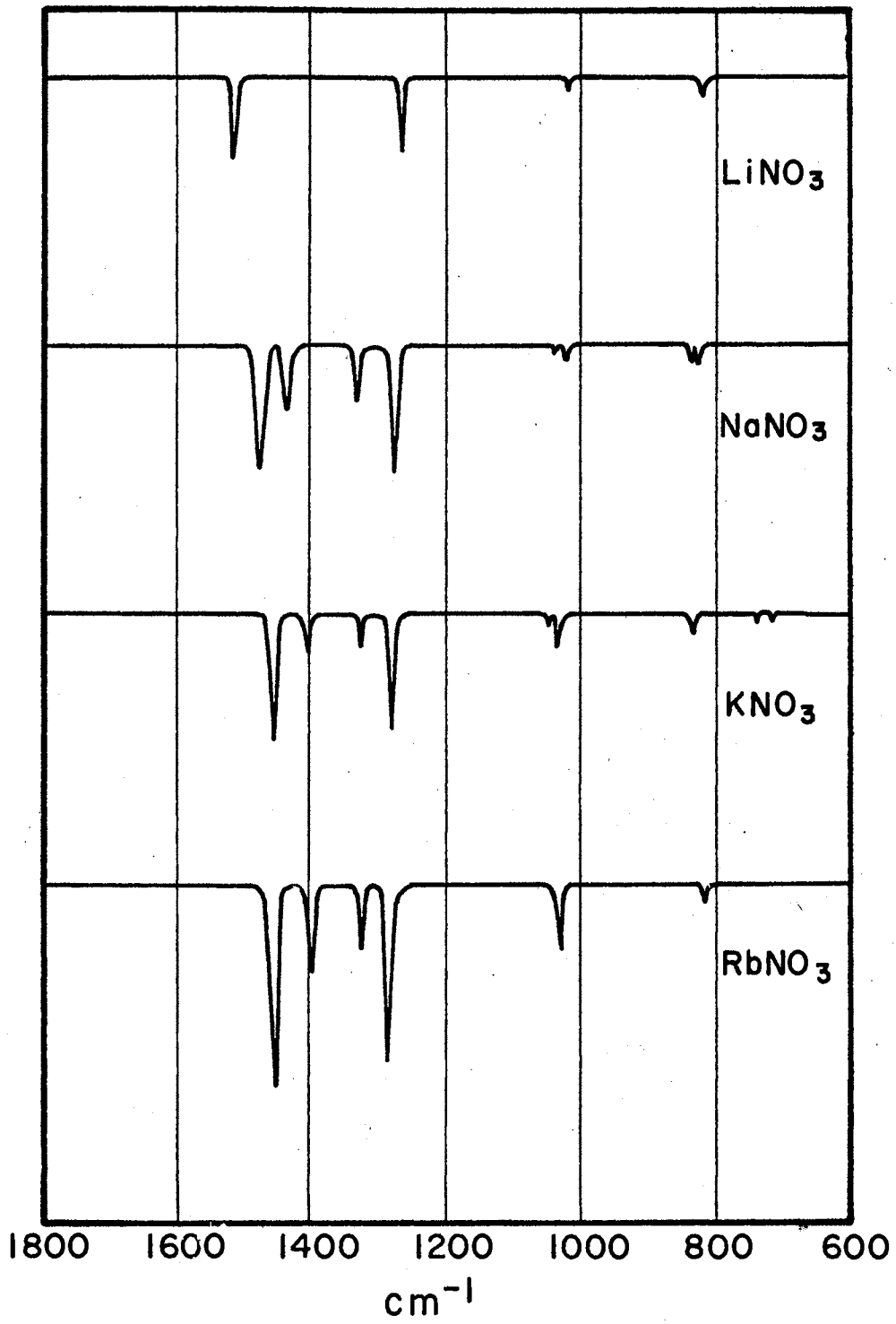

Figure 16. Infrared Spectra of Matrix-Isolated $LiNO_3$, $NaNO_3$, KNO_3, and $RbNO_3$

TABLE II

MONOMER FREQUENCIES FOR MATRIX-ISOLATED ALKALI-METAL NITRATES

Mode	$LiNO_3$	$NaNO_3$	KNO_3	$RbNO_3$
ν_1	1017	1023	1031	1033
ν_2	823	825	830	830
ν_{3a}	1275	1283	1291	1293
ν_{3b}	1515	1484	1462	1456

TABLE III

RESULTS FOR MONOMERS IN VARIOUS MATRIX MATERIALS

Mode	$LiNO_3$		$NaNO_3$			KNO_3		$RbNO_3$	
	CO_2	CCl_4	Ar	CO_2	Ar	CO_2	CCl_4	Ar	CCl_4
ν_1	1017	1015	1023	1023	1031	1035	1028	1033	1029
ν_2	823	--	825	826	830	829	--	829	--
ν_{3a}	1275	1266	1283	1284	1291	1295	1282	1293	1284
ν_{3b}	1515	1509	1484	1480	1462	1462	1437	1456	1430

minor differences are noted for different materials.

In Table IV are shown the results for the dimeric species. In general the ν_3 splitting is about half that of the monomer and ν_1 is shifted to higher frequencies, toward the solid state value. Where observable ν_2 is also shifted to higher frequencies.

Shown in Figure 17 is the spectrum of cupric nitrate and thallous nitrate. These results are tabulated in Table IV along with reported gas phase results for HNO_3.[35] The $Cu(NO_3)_2$ and $TlNO_3$ were chosen because of their large degree of covalency and high volatility. Since these are more covalent relative to the alkali-metal nitrates, we would expect a larger ν_3 split, approaching that of HNO_3. It is also apparent from the spectra that no dimer formation is evident. The mass spectrum of $Cu(NO_3)_2$ vapor has been observed[38], and no evidence for dimer formation was found. This is not an unexpected result considering the covalent nature of this compound.

An electron diffraction study of $Cu(NO_3)_2$ indicates that it is probably planar with four nitrate oxygen atoms surrounding the copper ion in a square array. This structure has a center of symmetry and belongs to the D_{2h} symmetry point group. The infrared spectrum is consistent with this model, although not inconsistent with other possibilities. In Figure 18 two other possibilities are shown. In all three cases coupling between the nitrate groups, evidenced by splitting of ν_{3a} and ν_{3b}, would not be detectable in the infrared spectrum. The additional data provided by the Raman spectrum of the gas phase or matrix isolated $Cu(NO_3)_2$ could easily distinguish between structures I and II or II and III but not between I and III. As in the alkali metal nitrates only ν_1 was observable at 985 cm^{-1}. This small shift from the

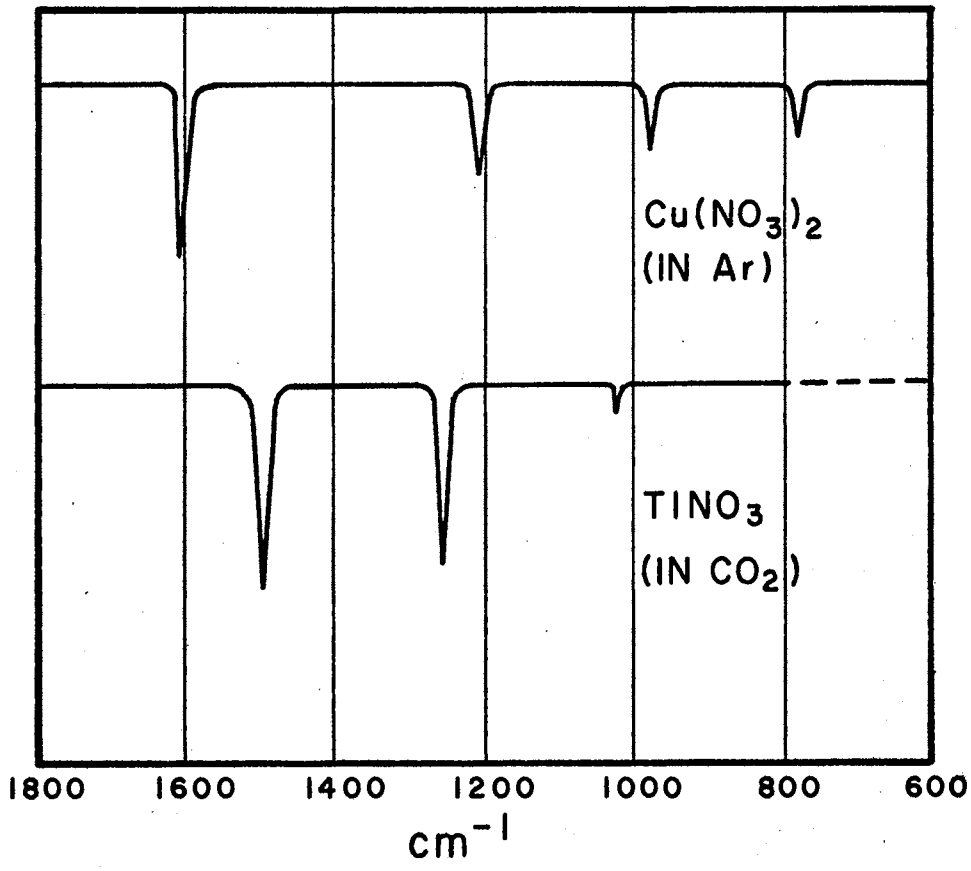

Figure 17. Infrared Spectra of Matrix-Isolated $Cu(NO_3)_2$ and $TlNO_3$

TABLE IV

FREQUENCIES FOR ISOLATED DIMERS

Mode	$NaNO_3$	KNO_3	$RbNO_3$
ν_1	1035	1053 (R) 1047 (IR)	1040
ν_2	835	835	835
ν_{3a}	1336	1337	1331
ν_{3b}	1440	1420	1415

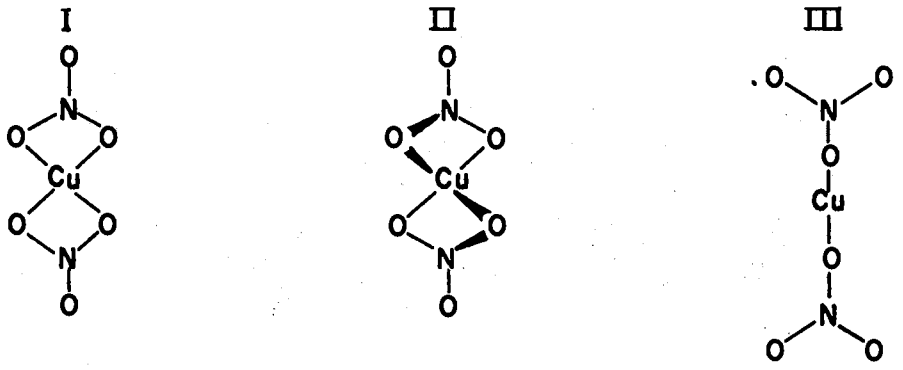

Figure 18. Three Possible Structures for $Cu(NO_3)_2$

I - square planar - D_2h - = $4A_g + 3B_{2g} + 2B_{3g} + Au + 4B_{1u} + 3B_{2u} + 4B_{3u}$

II - tetradhedral - D_{2d} - = $4A_1 + B_1 + 4B_2 + 6E$

III - linear - D_{2h} - = $4A_g + 2B_{2g} + 3B_{3g} + A_u + 4B_{1u} + 4B_{2u} + 3B_{3u}$

TABLE V

DATA FOR $Cu(NO_3)_2$, $TlNO_3$ AND HNO_3

Mode	$Cu(NO_3)_2$	$TlNO_3$	HNO_3[35]
ν_1	985 (R) 976 (IR)	1020	886
ν_2	785	----	765
ν_{3a}	1205	1252	1320
ν_{3b}	1615	1495	1710

infrared value is consistent with all three structures. It may be noted that the 410 cm^{-1} splitting for ν_3 in $Cu(NO_3)_2$ is rather large for a unidentate attachment of the nitrate groups as in structure III.

CHAPTER IV

FORCE CONSTANT ANALYSIS

A series of normal coordinate calculations were made on a model believed to closely represent the monomeric species. This was not necessarily to fit the observed frequencies to a set of force constants, but rather to estimate the changes in the force field necessary to cause the splitting observed in ν_3. From these results it may be possible to better understand the changes in bonding involved. Further it was desired to make a more detailed calculation on the contact-ion-pair model discussed by Wait, et al.[23] Though the results of their calculations have been used by several authors, there are several discrepencies in their derived force constants. Hence their results are of little use, as will be shown later. A brief calculation will be presented on a model embodying the features of the $Ag(NO_3)_2^-$ complex proposed by Devlin, et al. This model will also be used in a brief discussion of the $Cu(NO_3)_2$ spectrum.

Force Field

The Urey-Bradley force field was chosen because of its success in treating many various types of molecular systems, the ease in visualizing the physical meaning of the force constants involved, the transferability of force constants from one molecule to another, and the necessity for only a few parameters for a reasonably complete description of the po-

tential energy. The Urey-Bradley force field combines the features of the simple central and valence force fields. The potential energy is expressed as a sum of terms involving bond stretching (K) and bending (H) force constants as well as force constants between nonbonded atoms (F).

With the inclusion of the force constants listed above the basic Urey-Bradley force field can be expressed as follows:

$$2V = 2\Sigma_i K_i(\Delta r_i)^2 + 2\Sigma_j H_j(\Delta\alpha_j)^2 + \Sigma_k F_k(\Delta q_k)^2$$

$$+ 2\Sigma_i K_i' r_i \Delta r_i + 2\Sigma_j H_j'(\Delta\alpha_j) + 2\Sigma_k F_k' q_k \Delta q_k \qquad [1]$$

Where r_i is an equilibrium bond distance with associated stretching force constant K_i, α_j an equilibrium bond angle with associated bonding constant H_j, and q_k an equilibrium distance between non-bonded atoms with associated interaction constant F_k. Since this set of internal coordinates is not independent the linear terms in the expansion must be retained. In general the q_k can be related to the r_i and α_j by straightforward geometric substitutions so that the linear terms in r_i and α_k can be set equal to zero using the equilibrium conditions ($\frac{\partial V}{\partial r_i} = \frac{\partial V}{\partial \alpha_j} = 0$). The resulting potential energy expression then contains four types of force constants, K, H, F, and F'. On the basis that the nonbonded interactions are repulsive and proportional to $1/r^9$, F' is usually set equal to -0.1F. This is not always a valid assumption, but in any case F' is much smaller than F and in most cases the value of F' makes little difference in the results.[39,40]

The C_{2v} Model of the Contact-Ion-Pair

The geometry and force constant designations for the C_{2v} model are shown in Figure 19.

For a C_{2v} model we would expect the selection rules to be changed primarily by a splitting of the E modes, ν_3 and ν_4. The selection rules are listed in Table VI.

TABLE VI

CORRELATION TABLE FOR C_{2v} MODEL

D_{3h}		C_{2v}	Activity
ν_1 (A_1')	→	ν_2 (A_1)	IR, R (p)
ν_2 (A_2'')	→	ν_8 (B_2)	IR, R (d)
ν_3 (E')	→	ν_1 (A_1)	IR, R (p)
		$\{\nu_5$ (B_1)$\}$	IR, R (d)
ν_4 (E')	→	ν_3 (A_1)	IR, R (p)
		$\{\nu_6$ (B_1)$\}$	IR, R (d)
M--O stretching		ν_4 (A_1)	IR, R (p)
M--O planar bend		ν_7 (B_1)	IR, R (d)
M--O out-of-plane bend		ν_9 (B_2)	IR, R (d)

This table lists the complete set of selection rules. However, the calculation was restricted to the planar modes only (ν_1 - ν_7). The C_{2v} model was originally chosen for the melts by Wait, et al.[23], on the basis of the appearance of ν_1 in the infrared spectrum, ν_2 in the Raman spec-

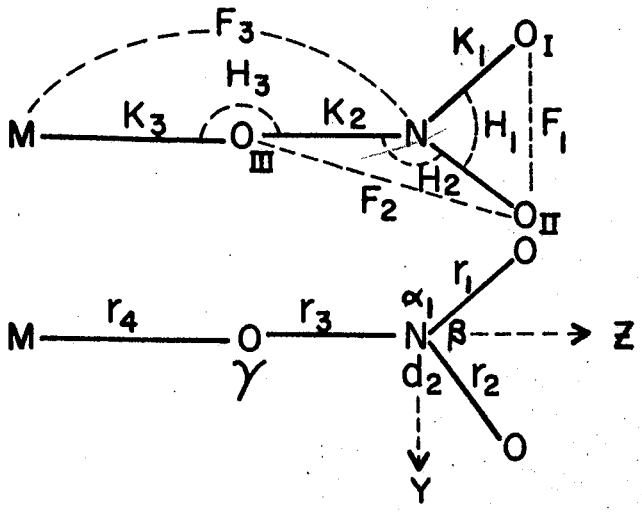

Figure 19. Geometry and Force Constants for MNO_3

trum, and the splitting of ν_3 with one branch in the Raman spectrum being polarized.

The initial calculation was made on $LiNO_3$. The force constants and geometric parameters were the same as those used by Wait, et al. These are listed in Table VII.

TABLE VII

FORCE CONSTANTS AND GEOMETRIC PARAMETERS FOR $LiNO_3$ AND $AgNO_3$

Geometric Parameters		Force Constants (Md/Å) $LiNO_3$	$AgNO_3$
$N\text{--}O_I = N\text{--}O_{III} = 1.22$ Å	K_1	6.170	5.853
$O_I\text{--}N\text{--}O_{II} = O_I\text{--}N\text{--}O_{III} = 120^\circ$	K_2	6.070	4.894
$M\text{--}O_{III}\text{--}N = 180^\circ$	K_3	0.384	0.894
$M\text{--}O_{III} = 1.70$ ($LiNO_3$)	H_1	0.518	0.558
$M\text{--}O_{III} = 2.31$ ($AgNO_3$)	H_2	0.608	0.579
	H_3	0.050	0.050
	F_1	1.530	1.574
	F_2	1.750	1.824
	F_3	0.050	0.050

A zero order calculation was made in an effort to duplicate the results of Wait, et al. As was anticipated, no agreement was obtained either for $LiNO_3$ or $AgNO_3$. A comparison of the results is given in Table VIII.

TABLE VIII

COMPARISON OF CALCULATED RESULTS FOR $LiNO_3$ AND $AgNO_3$

Mode	$LiNO_3$ WWJ	$LiNO_3$ This Calc.	$LiNO_3$ Difference	$AgNO_3$ WWJ	$AgNO_3$ This Calc.	$AgNO_3$ Difference
ν_1	1363	1415	52	1273	1331	58
ν_2	1067	1096	29	1039	1082	43
ν_3	726	679	-47	731	693	-38
ν_4	347	337	-10	188	189	1
ν_5	1440	1430	-10	1408	1397	-11
ν_6	724	708	-16	733	709	-24
ν_7	128	99	-29	93	63	-30

The primary point of disagreement is in the calculated splitting for ν_3. That the results of WWJ are inconsistent, if not entirely wrong, may easily be seen by comparing the amount of ν_3 splitting predicted with the difference in stretching force constants $K_1 - K_2 = \Delta K$. This comparison is shown in Table IX.

One expects the magnitude of the splitting to be primarily a function of ΔK, i.e., as ΔK approaches 0 the symmetry approaches D_{3h}, and the ν_3 splitting vanishes. From Table IX we see that the smallest reported ΔK is for $LiNO_3$, yet $\nu_5 - \nu_1$ is 79 cm^{-1} here, in distinct contrast to the rest of the alkali-metal nitrates. With the same force constants our calculation indicates a ν_3 splitting of only 15 cm^{-1}. In

TABLE IX

COMPARISON OF ΔK AND $\Delta\nu_3$ FROM WWJ[23]

Species	ΔK (Md/Å)	$\nu_5 - \nu_1$ (cm^{-1})
$LiNO_3$	0.103	79
$NaNO_3$	-1.099	2
KNO_3	-1.131	5
$RbNO_3$	-1.126	30
$CsNO_3$	-1.152	3
$AgNO_3$	.959	135
$TlNO_3$	- .370	46

order to get an 80 cm^{-1} splitting ΔK must be 1.6. In further support of our conclusions are the results of Brintzinger and Hester,[41] who made qualitative calculations on the magnitude of the force constant variations necessary to cause significant splittings of ν_3. Their results are in substantial agreement with ours, and, like our results, differ markedly with WWJ.

No further calculations were made for the purpose of describing the melt systems by a C_{2v} 1:1 contact-ion-pair model. It was felt that these results on $AgNO_3$ and $LiNO_3$ along with the results of Brintzinger and Hester were sufficient to invalidate the results of WWJ. Further in light of more recent data[27,29] it was concluded that the C_{2v} contact-ion-pair model is insufficient to account for all the features in the molten

nitrate spectra, and is probably not the dominant species in these systems.

$Ag(NO_3)_2^-$ Contact-Ion-Pair

Another contact-ion-pair model was postulated by Devlin, et al[42], to account for spectral features observed in molten $AgNO_3$. Impressed by the multiplicity of infrared and Raman features, and the lack of coincidence between their infrared band positions, and the Raman peak positions reported by Walrafen[43], Devlin, et al, were led to a more complex structure embodying a center of symmetry. A linear complex with two nitrate groups coordinated to one silver ion was proposed. This model was chosen because of the large number of vibrations expected, and the presence of a center of symmetry, so that the mutual exclusion principle applies. Vibrational assignments were made on the basis of this model, along with a perturbed lattice type of model.

In order to test the validity of this $Ag(NO_3)_2^-$ model, a zero-order calculation was made of the vibrational frequencies expected. Presented in Table X are the planar selection rules derived for this model and a partial listing of the suggested assignments.

In the absence of any vibrational coupling between the two nitrate groups, the frequencies of modes $\nu_1 - \nu_7$ will be identical to those of modes $\nu_8 - \nu_{14}$. For example, the only difference between ν_1 and ν_8 is a difference in the phase of the oxygen stretching motions. Hence the difference in the frequencies of ν_1 and ν_8 reflects the degree of coupling of the two nitrate groups. According to Devlin's assignment, this coupling results in a difference of 25 cm^{-1} between ν_1 and ν_8, 30 cm^{-1}

TABLE X

SELECTION RULES AND ASSIGNMENTS FOR THE $Ag(NO_3)_2^-$ MODEL

Mode	Symmetry	Activity
$\nu_1 - \nu_4$	A_g	Raman (p)
$\nu_5 - \nu_7$	B_{3g}	Raman (d)
$\nu_8 - \nu_{11}$	B_{1u}	Infrared
$\nu_{12} - \nu_{15}$	B_{2u}	Infrared

Raman[43]	Infrared[42]	Assignment
1420		ν_1 (A_g)
	1395	ν_8 (B_{1u})
1290		ν_5 (B_{3g})
	1260	ν_{12} (B_{2u})
1037		ν_2 (A_g)
	1025	ν_9 (B_{1u})

between ν_5 and ν_{12}, and 7 cm^{-1} between ν_2 and ν_9.

A calculation was made using force constants rather similar to those used in the C_{2v} calculation. No splittings nearly as large as those assumed were calculated for any reasonable set of force constants. In most cases the splittings were an order of magnitude less those observed. On the basis of these results it was concluded that the D_{2h} model was not a good representation of the predominant melt species.

The results obtained from this calculation have some relevance with

respect to $Cu(NO_3)_2$. Even though the model may not be a good representation of $Cu(NO_3)_2$, the degree of coupling between the nitrates should be fairly independent of the details of the model. Hence for $Cu(NO_3)_2$ we would not expect a large split for ν_1 and ν_8 or between ν_5 and ν_{12}. However, a splitting of ca. 10 cm^{-1} was calculated between ν_2 and ν_9 (the components derived from ν_1 in the free D_{3h} ion). A difference of ca. 10 cm^{-1} was observed between the infrared value for ν_1 and the Raman value for ν_1 for the isolated $Cu(NO_3)_2$ which is in qualitative agreement with the calculation.

C_{2v} Model of Monomer

A generalized calculation on a C_{2v} model was made in which the force constants K_1 and K_2 were varied over a large range of valves. This calculation is similar to that reported by Brintzinger and Hester.[41] A set of Urey-Bradley force constants was assumed for the "free ion", i.e., a D_{3h} force field which reproduced "free ion" frequencies. The nitrate bond-stretching force constants, K_1 and K_2, were then changed so that the bond to the coordinated oxygen was weakened, while the other two were strengthened. This situation is presumed to qualitatively represent simple polarization of the nitrate ion. This series of calculations was then repeated with a range of metal-oxygen force constants K_3. Since the mass of the metal atom makes little difference in the nitrate modes, a value of 30 AMU was used as more or less an average over the alkali-metal nitrates. Similarly, a metal-oxygen bond distance of 2.0 Å was assumed. The results of this calculation are plotted in Figure 20. From this it can be seen that polarization of the nitrate ion induces a rather large splitting in ν_3, and tends to lower ν_1. Increasing K_3 has

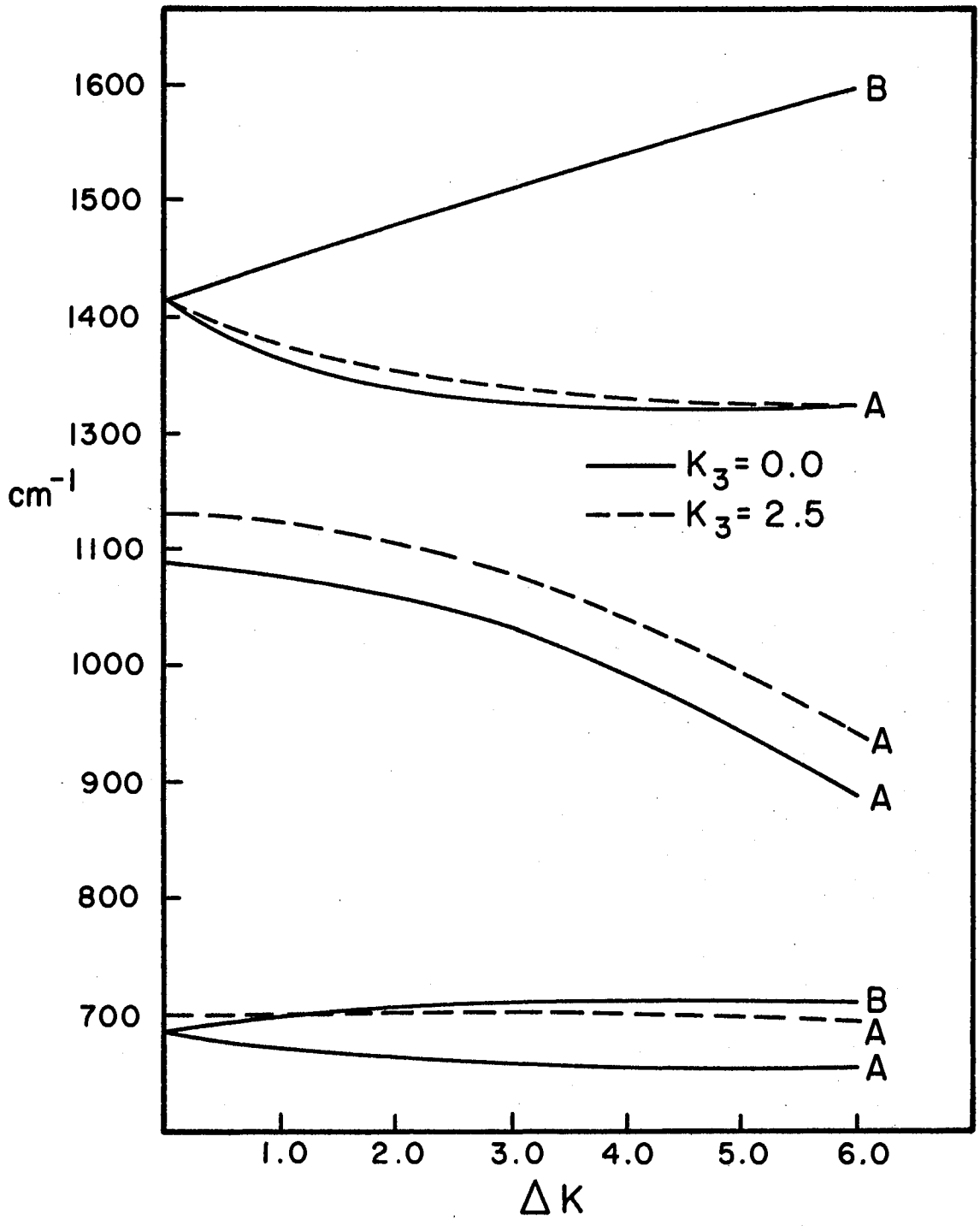

Figure 20. Variation of Calculated Planar Frequencies With ΔK

little effect on the splittings, but tends to raise ν_1. Hence the net result of these two effects would be to cause a large splitting in ν_3 and a gradual shift of ν_1 toward lower frequencies.

Shown in Figure 21 is a plot of observed frequencies for the isolated monomer vs. polarizing power of the cation. The polarizing power as defined by Janz and James[28] is

$$P = (Z/r)\ (5Z^{1.27}/rI)^{\frac{1}{2}} \qquad [2]$$

where r is the ionic radius, Z the ionic charge, and I is the ionization potential. The first term is the ionic potential, and the second a shielding factor. Although this definition is by no means rigorous, it should give a reasonable measure of the electrostatic polarization induced by the cation. Similar curves are obtained from a plot of e/r vs. frequencies. In any case the trends of the P vs. frequency plot are the same as the ΔK vs. frequency plot, indicating that the polarization effect is dominant.

From Figure 19 we can estimate the changes necessary to produce observed ν_3 splittings. These are tabulated in Table XI.

TABLE XI

VIBRATIONAL PARAMETERS FOR THE ALKALI-METAL NITRATES

M^+	$\Delta\nu_3$	P	K_1	K_2	ΔK	K_1/K_2
Li	240	1.84	7.57	2.87	4.70	2.63
Na	201	1.06	7.12	3.77	3.35	1.88
K	171	.756	6.87	4.27	2.60	1.60
Rb	163	.695	6.82	4.37	2.45	1.56

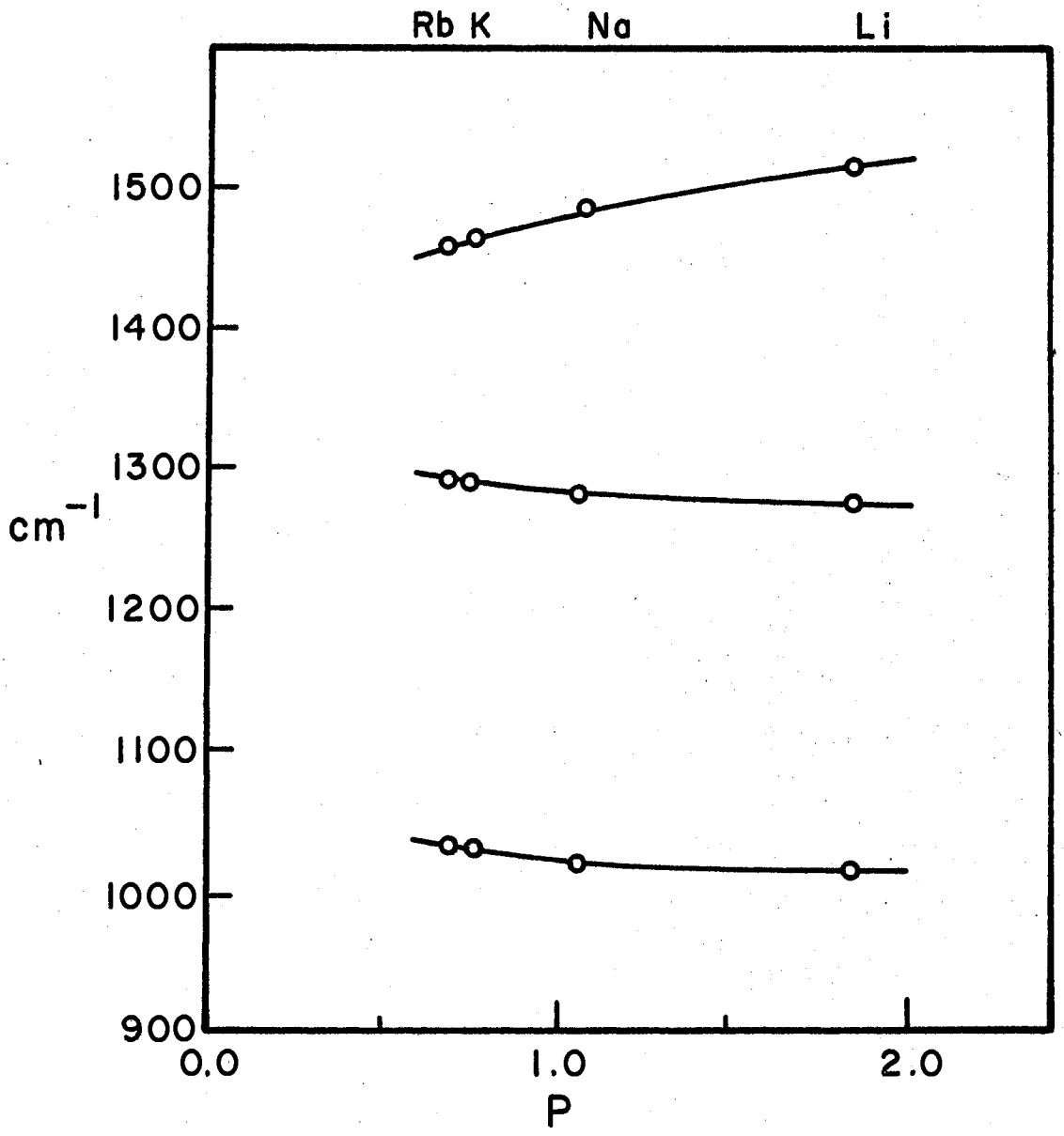

Figure 21. Variation of Observed Frequencies With Polarizing Power

Although the apparent linearity of ΔK and K_1/K_2 with P is probably fortuitous, it is in support of the dominant polarization thought to be present in the alkali-metal nitrates.

Isotope Calculation

A calculation was made on ^{15}N substituted nitrate to compare with the experimental results of ^{15}N labelled KNO_3. No attempt was made to fit the observed data. Table XII shows the calculated and observed shifts for the isolated monomer.

TABLE XII

^{15}N FREQUENCY SHIFTS

Shift	Calculated	Observed (KNO_3)
$\Delta\nu_1$	2.5	<1
$\Delta\nu_2$	----	21
$\Delta\nu_{3a}$	32.3	30
$\Delta\nu_{3b}$	32.6	31

CHAPTER V

SUMMARY AND CONCLUSIONS

Technique Evaluation

This research has been directed in part to the development of apparatus and procedures for the study of the Raman spectra of matrix isolated species. The efforts to this end can not be considered overwhelmingly successful. Although the single reflection technique is quite satisfactory for pure thin film investigations, it is not so successful for highly dilute films. If care is not taken to use pure materials and slow deposition rates, the resultant film will cause reflective scattering of the laser beam to such an extent that the signal-to-noise ratio is prohibitively low. Furthermore, the film may suffer enough local heating from the laser beam to cause diffusion of the active species such that effective isolation is destroyed. Attempts were made to use multiple reflection arrangements, but these were not successful. This is presumably due to the low thermal conductivity of the fused quartz multiple internal reflection plates used, resulting in poor quality deposits. However, this approach deserves further investigation.

In view of the difficulties involved in obtaining Raman spectra of matrix isolated species, it is gratifying that some results were obtained. The Raman spectra of the alkali-metal nitrate monomer provided no new information, but as was seen the Raman results on the dimer and $Cu(NO_3)_2$ monomer were quite informative.

Very good infrared spectra were obtained for the systems studied. These results were correlated with a series of normal coordinate calculations to obtain information on the nature of the isolated species. The significance of these results with respect to the structure of the monomer, dimer and melt systems is discussed below.

Monomer and Dimer Structural Properties

The structure of the monomer is probably planar and C_{2v}. However, the calculations are fairly insensitive to changes in the M-O-N angle. Hence no positive conclusion can be reached as to whether or not this bond is bent. The small variations in ν_2, the out-of-plane bending mode are indicative of a planar structure. The position of this band changes very little in going from Li to Rb. This mode was not included in the calculation because for a C_{2v} structure there is no coupling with the in-plane vibrational modes. If the monomer were not planar there would be coupling of ν_2 with some or all of the other modes and hence a dependence of the ν_2 frequency upon polarization and metal binding. That there is very little change observed in ν_2 implies little deviation from planarity for the monomer.

As discussed in conjunction with the calculations, the decrease in splitting in the Li to Rb series reflects the decrease in polarizing power of the ion, i.e., increase in ionic radius.

The structure of the dimer is not as clearly understood as is the monomer. The model discussed in Chapter III seems to be a reasonable one. The non-coincidence of ν_1 in the infrared and Raman are indicative of the presence of a center of symmetry and a weak coupling between the nitrate groups of the two monomers. As in the monomer case the relative-

ly small variation in ν_2 is supportive of a planar structure for the dimer. We may note from the dimer spectrum that the magnitude of the electrostatic polarization is considerably less in the dimer, as evidenced by the approximate halving of the ν_3 split relative to the monomer. This degree of change is not unreasonable considering that in the dimer each nitrate now has two weak N-O bonds and one strong one with the N-O bonds weakened only about half as much as for the corresponding interaction in the monomer. In other words the splitting for the dimer could be estimated by moving about halfway back on the ΔK axis in Figure 19. It can also be seen that this increases ν_1, which is consistent with observation.

The other two nitrate monomers studied, $TlNO_3$ and $Cu(NO_3)_2$ are not well described by the polarization interaction presumed to hold for the alkali-metal nitrates. The low melting points and high vapor pressures of $TlNO_3$ and $Cu(NO_3)_2$ are indicative of more covalent bonding in the solid. This higher degree of covalency would be expected to carry over to the vapor phase. As was shown in Table V the splitting is quite high relative to what would be expected on the basis of polarizing power alone. The observed splittings for $TlNO_3$ and $Cu(NO_3)$ are approaching that for HNO_3 or CH_3NO_3 which are known to be highly covalent. It may also be noted that dimer features are absent from the spectra. This results from the reduction in dipole strength in the covalent nitrates, relative to the ionic nitrates. Hence the dipole-dipole interaction is not sufficiently strong to promote formation of a stable dimer.

Vapor Composition

In the results presented, any possible thermal decomposition of the

various nitrate systems has been ignored. Possibly one of the reasons the nitrates have not been previously studied in the vapor is that they are presumed to decompose upon heating, rather than sublime. The usual mode of decomposition is thought to be[44]

$$2\ MNO_3 \rightarrow 2\ MNO_2 + O_2 \rightarrow MO_2 + NO_2 + NO.$$

However, the reaction products NO_2 and NO were observed only for $LiNO_3$. For the rest of the nitrates very little decomposition was indicated, and the major component of the vapor phase was found to be monomeric. For all of the alkali-metal nitrates a weak band was observed at 1215 cm^{-1} which shifted to 1185 cm^{-1} in the ^{15}N case. This band does not belong to NO_2 or NO, and no other peaks associated with it were detectable. Hence, its origin is presently not known.

A few diffusion experiments were performed in which the matrix was warmed to allow diffusion of the isolated species. In most cases monomer bands decreased and were replaced by the broad bands of the solid crystal. In $RbNO_3$ the monomer bands decreased while the dimer bands increased slightly. In the final stages of the diffusion process the dimer bands were replaced by the broad bands of the crystal. That the spectrum after diffusion showed no indication of the presence of nitrates, is good evidence that little decomposition occurred. This also precludes any confusion in spectral interpretation caused by interferences from isolated nitrates.

One of the reasons $Cu(NO_3)_2$ was chosen for investigation was its known high volatility. Mass spectrometric studies[34] have shown that it sublimes readily with little decomposition. Hence, it provides a good comparison for the alkali-metal nitrates. That the gross features ob-

served in the alkali-metal nitrate monomers are the same as for isolated $Cu(NO_3)_2$ is good evidence for arguing that the alkali-metal nitrates can also be sublimed without significant decomposition.

Correlation With Melt Spectra

This research was initiated with the hope of drawing some conclusions regarding the structures and/or interactions in the melt systems. In this respect the appearance of the dimer is fortuitous because more information can be inferred from its spectrum than from the monomer spectrum.

It was hoped to demonstrate that the ν_3 splitting observed in the infrared and Raman spectra of the molten nitrates is too large to be accounted for by cation distortion of the anion along. It is obvious that large distortions resulting in ν_3 splittings much larger than observed in the corresponding melts are present in the monomers (see Table XIII). However, this is in the very asymmetric field produced by one cation. In the dimer the amount of distortion is considerably reduced, resulting in ν_3 splittings comparable to the melt values. In the case of the melt though, the cation field is not expected to be nearly as asymmetric as the field experienced by the nitrates in the dimer. Hence, we would not expect the melt splitting to be nearly as large as the dimer splitting if such splitting were caused by distortion of the anion by the cation field. The same also holds true in the disordered solids, such as KNO_3 I, where the ca. 80 cm^{-1} split in ν_3 has been attributed to distortion splitting.[24]

Further evidence for a different mechanism operating in the melt systems may be inferred from the trends observed in ν_1 for the two dif-

ferent cases. Through the monomeric alkali-metal nitrates we see that ν_1 increases as the ν_3 splitting decreases. In the molten systems however ν_1 decreases through the alkali-metal series much as for the solid state. Further the change in ν_1 going from solid to liquid is quite small, whereas the crystalline to monomer change is quite large. A similar comparison exists for the dimer. These and other observations are presented in Table XIII. Whatever conclusions we draw from this comparison, it is suggested that anion distortion via cation electrostatic interaction is probably not important in the melt. Hence, we can conclude that the ion-pair description of the melt is not realistic. Also any quasicrystalline model in which there is embodied a large (ca. 100 cm^{-1}) site splitting for ν_3 may be considered a doubtful representation.

The results of this study present little positive evidence to substantiate the ν_3 splitting mechanism recently proposed by Devlin, et al.[30,31] However, by this model the observed splitting in ν_3 arises from a TO - LO splitting of the ν_3 phonon in an analogous manner to the crystatline phase.

Although some degree of site splitting of ν_3 is not entirely precluded by this model, the gross features are explained on the basis of a largely unperturbed nitrate ion. Hence, the contribution of this research to the nature of the melt systems has been in the form of negative inferences. It can be concluded that some models of the molten state are not realistic, but no particular agreement or disagreement with the model of Devlin, et al. can be inferred from these results.

TABLE XIII

COMPARISON OF MATRIX-ISOLATION RESULTS WITH MELT AND SOLID DATA

	$LiNO_3$				$NaNO_3$			
Mode	Monomer	Dimer	Melt	Solid	Monomer	Dimer	Melt	Solid
1	1017	----	1061	1073	1023	1035	1055	1069
2	823	----	827	837	825	835	833	835
3a	1275	----	1361	1353	1283	1336	1345	1353
3b	1515	----	1478	1470	1484	1440	1425	1455
	KNO_3				$RbNO_3$			
1	1031	1053 1047	1045	1050	1033	1040	1046	1052
2	830	835	829	804,821	829	----		812,833
3a	1291	1337	1350	1350	1293	1331	1340	1340
3b	1462	1420	1410	1440	1456	1415	1405	1407

CHAPTER VI

SUGGESTIONS FOR FURTHER WORK

As was noted in the discussion, further techniques need to be explored for the study of Raman spectra of matrix isolated species. It has been demonstrated recently at Bell Laboratories that by using appropriate prism and thin film combinations, a laser beam can be trapped within a solid film. Perhaps a variation of this technique could be adapted for matrix isolation work.

The investigation of the matrix isolated nitrates brings up a number of interesting questions. The dimer structure is only qualitatively understood. Hence further investigation with emphasis upon the dimer is warranted. A mass spectrometric study of the alkali-metal nitrate vapors as a function of temperature might lead to the appropriate temperature for the formation of a maximal proportion of the dimeric species. More extensive Raman data on the dimer would be of considerable value.

Even though the alkali-metal nitrates are highly ionic, this study has shown that they can be vaporized without serious decomposition. A thorough mass spectrometric study should be of value in identifying the proper products and/or mechanism of decomposition at higher temperatures. The matrix-isolation technique could also be utilized to study other oxyanions, such as, ClO_3^-, ClO_4^-, etc.

As was reported in the results, the low frequency stretching and

bending modes were not observed, presumably because of the inherent low intensity of these modes and/or the low sensitivity of the infrared instrumentation. With greater film thickness and better instrumentation, perhaps these modes would be detectable.

The overall effect of changing from Ar to CO_2 as a matrix material was seen to be negligible. However, the relative intensities of the matrix-split components of the individual bands were seen to change considerably (see Figure 15). It was not determined whether this change resulted entirely from matrix effects, or whether part of this change was due to temperature effects. A study of this splitting as a function of temperature would provide insight into the question of whether this splitting arises from multiple site effects or hindered rotational effects.

A SELECTED BIBLIOGRAPHY

1. Pimentel, G. C., Dows, D. A. and Whittle, E., J. Chem. Phys. 22, 1943 (1954).

2. Andrews, L., J. Chem. Phys. 48, 972 (1968).

3. Andrews, L., J. Chem. Phys. 48, 979 (1968).

4. Pimentel, G. C. and Brown, H. N., J. Chem. Phys. 29, 883 (1958).

5. Olgilvie, J. F., Spectrochim. Acta 23A, 737 (1967).

6. Milligan, D. E. and Jacox, M. E., J. Chem. Phys., 38, 2627 (1963).

7. Milligan, D. E. and Jacox, M. E., Applied Optics, 3, 873 (1964).

8. Pimentel, G. C., Pure Appl. Chem. 4, 61 (1962).

9. Pimentel, G. C., Spectrochim. Acta, 12, 94 (1958).

10. Hallam, H. E., in "Molecular Spectroscopy", Proceedings of the 4th Institute of Petroleum Hydrocarbon Research Conference, 1968, 329, Institute of Petroleum, London.

11. Mann, D. E., Colder, G. V., et al., J. Chem. Phys., 46, 1138 (1967).

12. Weltner, W. and Warn, J. R., J. Chem. Phys., 37, 292 (1962).

13. Pitzer, K. S. and Snelson, A., J. Phys. Chem., 67, 882 (1963).

14. Van Thiel, M., Becker, E. D. and Pimentel, G. C., J. Chem. Phys., 27, 95 (1957).

15. Van Thiel, M., Becker, E. D. and Pimentel, G. C., J. Chem. Phys., 27, 486 (1957).

16. Levin, I., Spectrochim Acta, 25A, 1157 (1969).

17. Alfano, R. R., App. Optics, 8, 2095 (1969).

18. Janz, G. J. and Mikawa, Y., J. Mol. Spectry., 5, 92 (1960).

19. Mathieu, J. and Lounsbury, M., Disc. Far. Soc., 9, 196 (1950).

20. Vollmar, P. M., J. Chem. Phys., 39, 2236 (1963).

21. Irish, D. E. and Davis, A. R., Can. J. Chem., 46, 943 (1968).

22. Hester, R. E. and Plane, R. A., J. Chem. Phys., 40, 411 (1964).

23. Wait, S. C., Ward, A. T., and Janz, G. J., J. Chem. Phys., 45, 133 (1966).

24. Chisler, E. V., Soviet Physics-Solid State, 11, 1032 (1969).

25. James, D. W., Private Communication.

26. Smith, G. P., Molten Salt Chemistry, ed. Blander, M., Interscience, New York, 1964, p. 427.

27. Devlin, J. P., Williamson, K., and Li, P. C., J. Chem. Phys., 48, 3891 (1968).

28. Janz, G. S. and James, D. W., J. Chem. Phys., 35, 739 (1961).

29. James, D. W. and Leong, W. H., J. Chem. Phys., 51, 640 (1969).

30. Devlin, J. P., Pollard, G. and Frech, R., J. Chem. Phys., 53, 000 (1970).

31. Devlin, J. P., James, D. W., and Frech, R., J. Chem. Phys., 53, 000 (1970).

32. White, G. K., Experimental Techniques in Low Temperature Physics, Oxford University Press, Oxford, 1959.

33. Addison, C. C., and Hathaway, B. J., Proc. Chem. Soc., 1958, 3099.

34. Porter, R. F. and Schoonmaker, R. C., J. Chem. Phys., 29, 1070 (1958).

35. Pitzer, K. S. and Snelson, A., J. Chem. Phys., 67, 882 (1963).

36. Ferraro, D. R. and Walker, A., J. Chem. Phys., 42, 1273 (1965).

37. Marcus, R. A. and Fresco, J. M., J. Chem. Phys., 27, 564 (1957).

38. Porter, R. F., Schoonmaker, R. C., and Addison, C. C., Proc. Chem. Soc., 1959, 11.

39. Devlin, J. P., J. Chem. Phys., 39, 2385 (1963).

40. Devlin, J. P., J. Chem. Phys., 41, 2951 (1964).

41. Hester, R. E. and Brintzinger, H., Inorg. Chem., 5, 980 (1966).

42. Devlin, J. P., Williamson, K., and Austin, G., J. Chem. Phys., 44, 2203 (1966).

43. Walrafen, G. E. and Irish, D. E., J. Chem. Phys., 40, 911 (1964).

44. Sidgwick, N. V., Chemical Elements and Their Compounds, Oxford University Press, Oxford, 1950.

VITA[v]

Donald Eugene Smith

Candidate for the Degree of

Doctor of Philosophy

Thesis: A VIBRATIONAL STUDY OF A SERIES OF MATRIX-ISOLATED NITRATES

Major Field: Chemistry

Biographical:

Personal Data: Born in Alice, Texas, September 30, 1944, the son of Charles C. and Lennie P. Smith.

Education: Graduated from Batesville High School, Batesville, Arkansas, in May, 1962; attended Arkansas College, Batesville, Arkansas, from 1962 to 1965; transferred to Oklahoma State University in 1965, and received the Bachelor of Science degree with a major in Chemistry in 1966; completed the requirements for the Doctor of Philosophy degree in May, 1971.

Professional Experience: National Science Foundation Undergraduate Research Participant, Summer, 1964, and Summer, 1965; Graduate Teaching Assistant, Oklahoma State University, 1966 and 1967; National Aeronautics and Space Administration Trainee, 1966, and 1967; National Science Foundation Trainee, 1969 and 1970.